Investigations on Autogeneous Joining of Thin Stainless Steel Sheets by Pulsed Micro Plasma Transferred Arc

A THESIS

Submitted in partial fulfillment of the requirements for the award of the degree

of

Master of Technology

in

Mechanical Engineering

with specialization in

Production and Industrial Engineering

by

Jigar Chaudhary

DISCIPLINE OF MECHANICAL ENGINEERING

INDIAN INSTITUTE OF TECHNOLOGY INDORE

JUNE 2015

INDIAN INSTITUTE OF TECHNOLOGY INDORE

CANDIDATE'S DECLARATION

I hereby certify that the work which is being presented in the MTech thesis entitled **"Investigations on Autogeneous Joining of Thin Stainless Steel Sheets by Pulsed Micro Plasma Transferred Arc"** in the partial fulfillment of the requirements for the award of the degree of **MASTER OF TECHNOLOGY** in **MECHANICAL ENGINEERING** with specialization in **PRODUCTION and INDUSTRIAL ENGINEERING** and submitted in the **DISCIPLINE OF MECHANICAL ENGINEERING** at **INDIAN INSTITUTE OF TECHNOLOGY INDORE**, is an authentic record of my own work carried out during the time period from May 2014 to June 2015 under the supervision of **Prof. Neelesh Kumar Jain** and **Prof. Satish Chandra Koria** of Discipline of Mechanical Engineering.

The matter presented in this thesis has not been submitted elsewhere by me for the award of any other degree.

Jigar Chaudhary

This is to certify that the above statement made by the candidate is correct to the best of our knowledge.

Prof. Neelesh Kumar Jain **Prof. Satish Chandra Koria**

Jigar Chaudhary has successfully passed his M.Tech. Oral Examination, held on**...........**

Signature of M.Tech. Thesis Supervisors
Date:

Convener, DPGC
Date:

Signature of PSPC Member 1
Date:

Signature of PSPC Member 2
Date:

Signature of Chairman, Oral Examination Board with date

ACKNOWLEDGEMENTS

This thesis is a result of research carried out at Indian Institute of Technology, Indore. During this period, I came across people who supported and helped me and in my research in various ways and would thereby take this opportunity to thank them and their incredible support for my work. It is my great pleasure to convey my gratitude to all of them.

First, I would like to thank and acknowledge to **Prof. N. K. Jain** for his advice, interest and encouragement during the course of this research work. It was through his guidance and our many hours of discussion that led to the successful completion of this work. His guidance throughout my graduate academic career has been invaluable and is greatly appreciated.

I would also like to thank to **Prof. S. C. Koria** for his invaluable suggestions. This work would not have been possible without the encouragement and expert guidance of my supervisors. Their enthusiasm and optimism made this experience both rewarding and enjoyable. Most of the novel ideas and solutions found in this thesis are the result of our numerous stimulating discussions. Their feedback and editorial comments were also valuable for writing this thesis. I feel lucky to have got an opportunity to work under them. Not only understanding the subject, but also interpreting the result drawn there on from the graphs was very thought provoking.

Feedback and help by Post-Doctoral Fellow **Dr. Suyog Jhavar** during preparation this of thesis is sincerely acknowledged. A special acknowledge to lab staff Rishi Raj and Deepak Rathode and Pavendra Muchal for their efficient work. And last but not the least I would like to thank God and my parents for providing me with opportunities throughout the life.

Jigar Chaudhary

Dedicated to my Parents

ABSTRACT

There are wide varieties of applications of thin sheets (thickness < 2 mm) in day-to-day life. Some of the applications of thin sheets are: air plane fuselages skin (2 mm), automobile body panels (1 mm), duct works (0.45 to 2 mm), sheet bellows (0.15 mm) etc. Joining of thin sheets is very challenging due difficulty in maintaining the localized melting and subsequent solidification. This is compounded while joining thin sheets of stainless steel due to its poor weldability. This thesis is focused on autogeneous joining of thin (0.4mm thickness) sheets of AISI 316L austenitic stainless steel using pulsed micro plasma transferred arc process. Effects of pulse-on time, pulse-off time, peak current and torch travel speed were investigated to determine their optimum levels for joint tensile strength and its microstructure. To evaluate the effects of the input variable parameters on the joint strength, analysis of variance (ANOVA) with a confidence interval of 95% was done. Based on ANOVA results, contribution of each process parameter and their interaction on the joint strength was evaluated. It also provides an indication of which process parameters are statistically significant.

It was found that 50% duty cycle, 10% pulse frequency, 3.5 A peak current and torch travel speed 250 mm/min yielded maximum joint strength 553 MPa. The fusion zone was found to have finer grain size. Absence of heat affected zone was confirmed by very small variation in Vickers microhardness values across the fusion zone. This study establishes capability of pulse micro plasma transferred arc process for joining thin sheets of stainless steel without any filler material and producing very good quality joint using much less power as compared to conventional fusion joining processes.

PUBLICATION

1. J. Chaudhary, N. K. Jain, S. C. Koria, "On Autogeneous Joining of Thin Stainless Steel Sheets by Pulsed Micro Plasma Transferred Arc Process", **Materials and Manufacturing Processes** (under review since 3rd June 2015; Manuscript ID: LMMP-2015-0718) **(Impact Factor: 1.629)**

CONTENTS

LIST OF FIGURES

LIST OF TABLES

NOMENCLATURE

$\boldsymbol{I_p}$ Peak current (A)

$\boldsymbol{I_b}$ Base current (A)

$\boldsymbol{f}$ Pulse frequency (Hz)

τ Duty Cycle (%)

$\boldsymbol{f_p}$ Plasma gas flow rate (lpm)

$\boldsymbol{f_s}$ Shield gas flow rate (lpm)

$\boldsymbol{V_t}$ Torch travelling speed (mm/min)

$\boldsymbol{X}$ Stand-off distance (mm)

$\boldsymbol{T_{on}}$ Pulse-on time (s)

$\boldsymbol{T_{off}}$ Pulse-off time (s)

Organization of the Thesis

This thesis is organized into FIVE chapters with following contents:

Chapter 1 details applications of thin sheets, challenges in joining of thin sheets with particular reference to stainless steel thin sheets, different joining processes for thin sheets, concept of the pulsed micro-plasma transferred arc (P-μPTA) process, its parameters, advantages and limitations.

Chapter 2 presents review of past work on thin sheet joining using different joining processes, research gaps identified based on this review and the research objectives defined based on the identified research gaps.

Chapter 3 describes planning and details of experiments carried out for the present work. It presents details of the different sub-systems and the components used in the development of the experimental apparatus and preliminary experimental planning to bracket parameters affecting joint strength during SS316L thin sheet joining. It also presents the various results of preliminary experiments and bracketed range for main experiments.

Chapter 4 presents experimental results and their analysis focusing on the effects of variable input parameters of P-μPTA process joint strength of SS thin sheets along with identification of optimum level of the process parameters. It also presents analysis of the optical micrographs and microhardness to study HAZ of the optimal joint. Analysis of variance is employed to determine the significant parameter.

Chapter 5 highlights the conclusions derived from the present work and scope for future work based on the limitations of the present work.

Chapter 1

Introduction

Sheets having thickness up to 2 mm are referred as thin sheets. They are frequently used to provide good strength with reduced weight. Joining thin sheets is very difficult and challenging as compared to joining of thick sheets because of difficulty in maintaining a localized melting and solidification zone due to high surface area to volume ratio of thin sheets. Due to higher amount of heat involved, use of conventional fusion arc joining processes results in defects such as burn through, large heat affected zone (HAZ), warping, buckling and twisting of sheets, grain coarsening, oxide formation and reduction of important elements introduced in the coatings of thin sheets. These problems become more compounded while joining stainless steel (SS) thin sheets due to its poor weldability. Selection of proper joining process, procedure and optimization of process parameters can solve these problems to a large extent.

Stainless steel is broadly classified into five different types: Ferritic, Martensitic, Austenitic, Duplex and Precipitation Hardened (PH). Among these five different types, austenitic stainless steels have excellent corrosion-resistant and most widely used in food processing equipment, chemicals and fertilizer containers, heat exchangers, ducts, etc. applications. Austenitic stainless steels are characterized by their high strength, excellent toughness, good corrosion resistance combined with resistance to stress corrosion cracking and corrosion fatigue. Chromium and molybdenum present in the austenitic stainless steel enhance their resistance to corrosion. Austenitic Stainless steel alloys contain minimum 10.5% chromium and this forms a protective self-healing oxide film which has their characteristic "stainlessness" or corrosion resistance. Present work is concerned with the austenitic stainless steel thin sheets.

In the fabrication of SS products, components, or equipment, manufacturers generally employ welding as the principal joining method. However, stainless steels may undergo certain changes during welding. It is necessary, therefore, to exercise a reasonable degree of care during welding to minimize or prevent any deleterious effects that may occur, and to preserve the same degree of corrosion resistance and strength in the weld zone that is an inherent part of the base metal. These difficulties are even more compounded with the thin sheets.

1.1 Applications of Stainless Steel Thin Sheets

Stainless steel thin sheets are used in various industrial applications such as fuselages skin of an airplane (2 mm), automobile body panels (1 mm), duct works (0.45 to 2 mm), sheet bellows (0.15 mm) etc. Some of the applications of thin sheets are shown in Fig. 1.1.

(a)

(b)

(c)

(d)

Fig. 1.1: Thin sheet applications (a) Boeing 747 fuselages skin (thickness 1.8-2.2 mm); (b) Automobile body panel parts (thickness 1mm); (c) Bellows sheet (thickness 0.15 mm); (d) Duct work (0.45-2.0 mm).

1.2 Problems in Joining of Thin Sheets

Most of the problems encountered during the joining of thin sheets are generally found to be linked with large amount of heat input with conventional welding techniques. High heat generated leads to a large number of problems in thin sheet joining including burn through or melt through, distortion, porosity, buckling, warping and twisting of joined sheets, grain coarsening, evaporation of useful elements presents in the coating of the sheets, oxide formation on grain boundary, joint gap variations during joining, fume generation from the coated sheets etc. Some of the problems are shown in Fig. 1.2

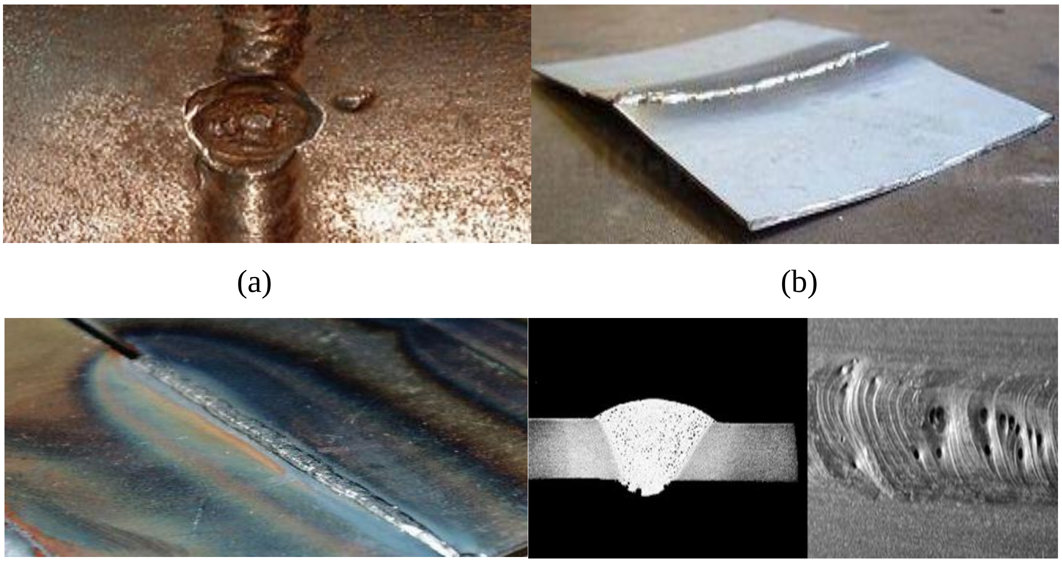

(a) (b)

(c) (d)

Fig. 1.2: Problems with thin sheets joining (a) burn through, (b) buckling, (c) large heat affected zone, and (d) porosity.

1.2.1 Problem with Joining of Austenitic SS Thin Sheets

Joining austenitic stainless steel is very challenging because of their lower thermal conductivity (16.3 W/mK) and high coefficient of thermal expansion (16 x 10^{-6} per ^{o}C) in comparison to Al and Cu based alloys. Both these properties govern thermal distortions and internal stresses which increase susceptibility of the joint to hot cracks. In the temperature range from 540 to 850 ^{o}C, chromium carbide is formed along with austenite grains. This causes depletion of chromium from the grains decreasing the corrosion protective passive film. This effect is called sensitization.

1.3 Various Joining Processes

The process of permanent joining two materials (usually metal) through localized coalescence resulting from a suitable combination of temperature, pressure and metallurgical conditions is termed as welding. It can be achieved by using heat or pressure or both with or without use of addition metal at the interface. Depending upon the combination of temperature and pressure, many joining processes have been developed. Based on the state of joining, the joining processes can be broadly classified as: (i) Liquid state welding (Fusion welding), (ii) Solid/liquid state welding and (iii) Solid state welding. Fig. 1.3 presents classification of various joining processes.

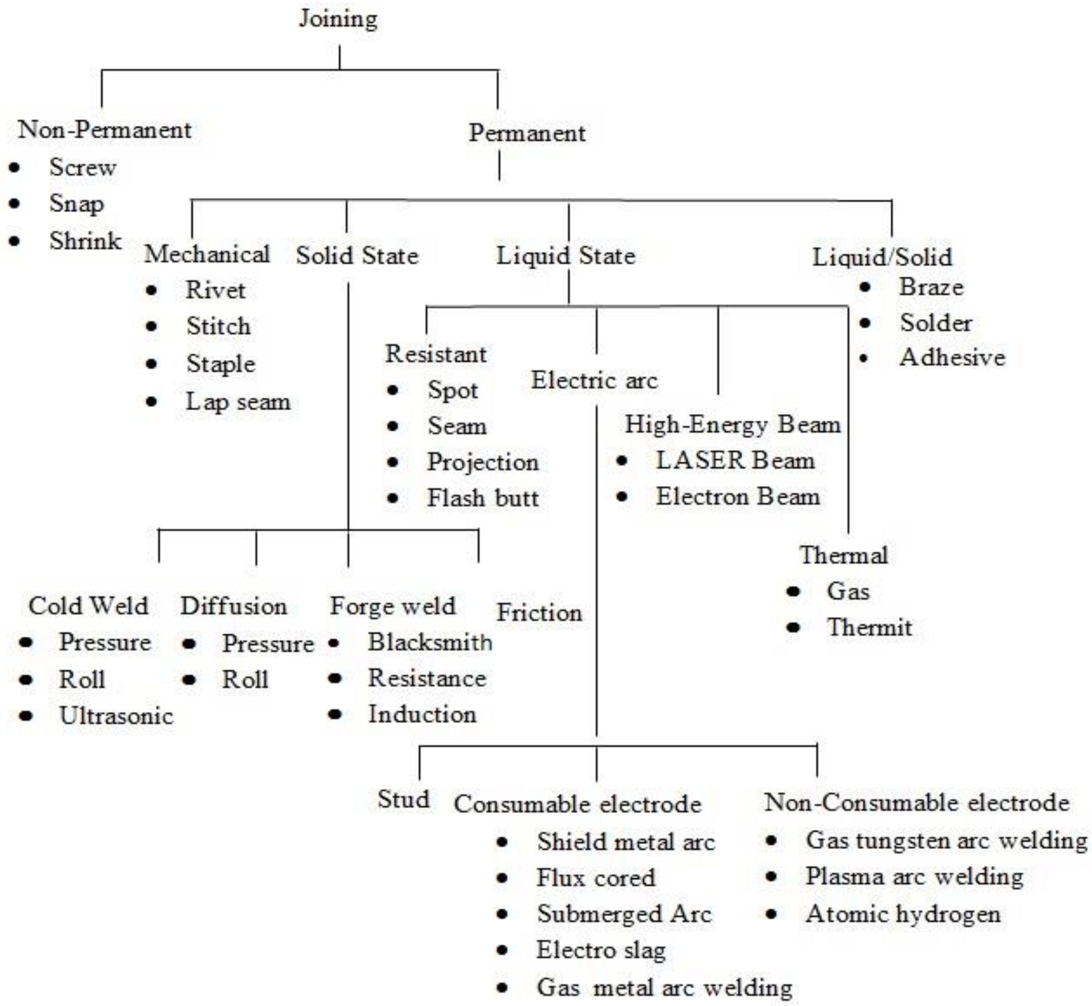

Fig. 1.3: Various joining processes.

1.4 Joining Processes for Thin Sheets

Five welding processes have been explored to meet the challenges of joining the thin sheets. They are continuous and pulsed version of gas metal arc welding (GMAW), gas tungsten arc welding (GTAW), laser beam welding (LBW), pulsed version of electron beam welding (EBW) and micro-plasma transferred arc welding (P-µPTAW) processes. Table 1.1 summarizes the comparative evaluation of these five thin sheet joining processes. Gas metal arc welding (GMAW), also known as metal inert gas (MIG) welding, uses filler material in the form of wire as an electrode. It uses high current which results high distortion, blotchy holes and porosity. In the pulsed version of gas tungsten arc welding (GTAW), also known as tungsten inert gas (TIG) welding, a high voltage, high-frequency pulse starts an electric arc between a tungsten electrode and the parts to be joined. The intense heat of arc fuses the materials with or without filler material. An inert shield gas provides a conductive ionized path to the workpiece surface and protects the tungsten electrode and molten material from oxidation. Shield gases include argon, helium or mixture of hydrogen and argon whose selection is done according to type of the material being joined. Electron beam welding (EBW) uses a high velocity jet of electrons focused at the joint to be welded in a vacuum chamber. Therefore, it tends to be expensive and requires longer setup times. Laser beam welding (LBW) employs heat from a focused coherent monochromatic light (i.e. laser) beam to fuse the materials to be joined. During this process, it is essential to accurately position the weld joint and maintain the joint gap. Micro-plasma transferred arc welding (μ-PTAW) process uses thermal energy obtained from the plasma generated by ionization of an inert gas. Recent advances in power supply and control over process parameters (i.e. current value as low as 0.1A and pulse duration up to 0.01 sec) enable this process to produce extremely accurate welds with very low heat input. Therefore, chances of tungsten inclusion, difficulty in starting the arc by touching, HAZ and thermal distortion are almost eliminated in this process. This process gives better weld quality than pulsed GTAW, LBW and EBW and is much economical.

Table 1.1: Comparative study of different joining processes for thin sheets.

Parameter	**Gas metal arc welding (GMAW)**	**Gas tungsten arc welding (GTAW)**	**Laser beam welding (LBW)**	**Electron beam welding (EBW)**	**Micro-plasma transferred arc welding (μ-PTAW)**
Heat source	Arc by short circuiting	Arc by short circuiting	Focused coherent monochromatic light beam	Focused high velocity jet of electrons	Heat from the plasma
Operation mode	Continuous or pulsed	Continuous or pulsed	Continuous or pulsed	Pulsed (frequency as low as 50 μs)	Continuous or pulsed
Arc density	Moderate	High	High	Very high	High
HAZ	Larger than GTAW	Medium	Small	Very small	Small
Deposition efficiency	90-95%	up to 99%	up to 99%	up to 99%	up to 99%
Magnetic influence	Causes arc blow	Causes arc blow	No influence	No influence	Causes arc blow
Cost	Moderate to high	Moderate	Very high	Extremely high due to vacuum requirement	Expensive than GMAW and GTAW but cheaper than LBW and EBW
Uses	For small volume production	For small volume production	For large volume production	Not for commercial purposes	For medium volume production

Pulsed GTAW and μ-PTAW are probably the two most commonly used methods for precision joining of thin sheets. Both methods can be a low-cost alternative to EBW and LBW.

1.4.1 Joining Using Pulsed Power

In the liquid state joining processes, only melting and fusing the materials to be joined would not result in joining the work materials unless sufficient time for the solidification of the molten and fused material is allowed. One major breakthrough in joining processes is the use of pulsed power after realizing that use of continuous power supply causes higher heat input which does melting but does not provide sufficient time for solidification of the fused materials resulting in burn-through rather than joining. While using continuous power supply in these joining processes, a skilled welder 'weaves' his hand by oscillating so that the melt time is synchronizes with solidification time. This skill is electronically mimicked in using pulsed arcs, which lowers the heat input little bit into the heat sensitive arc zone and helps a less skilled joiner to produce better quality joints. Use of pulsed arc is must while joining the thin sheets due their smaller thickness and large surface area to volume ratio which causes problem of burn-through more frequently than that in case of thick sheet joining.

1.4.2 Pulse-Micro Plasma Transferred Arc Welding (P-μPTAW)

Plasma transferred arc welding (PTAW) is advancement over the GTAW process and can be used to join all the material that are joinable with GTAW (i.e. most commercial metals and alloys). This process is characterized by higher precision, better stability, highly concentrated arc, narrow and clean weld, smaller HAZ and longer operation time of the electrode. Main difference between the PTAW and the GTAW processes is the positioning of the electrode within the body as shown in Fig. 1.4. In the GTAW process, the electric arc is formed between the tungsten electrode and workpiece while in PTAW process a pilot arc is formed between the tungsten electrode and the constricting copper nozzle placed inside the torch.

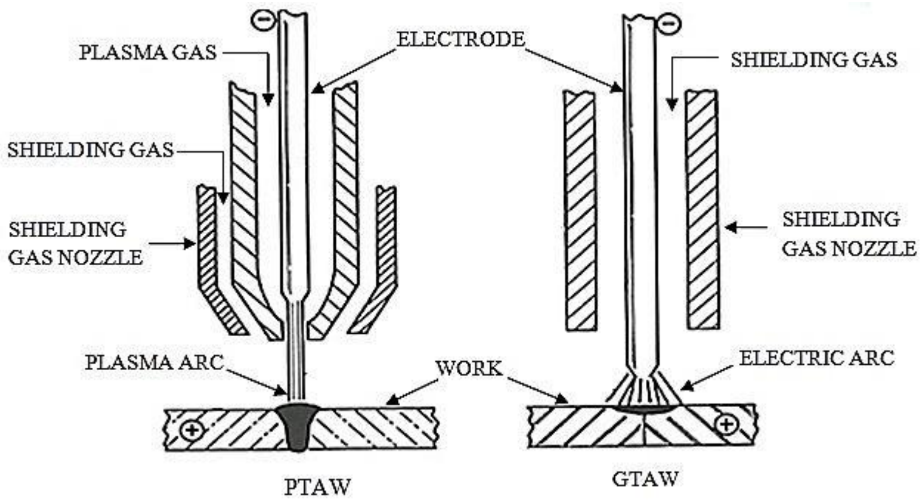

Fig. 1.4: Working principle of PTAW and GTAW processes.

There are two gases used in the PTAW process to perform different functions:

(1) Plasma gas: for generating plasma between the tungsten electrode and the constricting nozzle.

(2) Shielding gas: to protect the weld from the atmosphere and oxidation.

PTAW torch is provided with two independent power circuits i.e. for (i) pilot arc, and (ii) main arc. Fig. 1.5 depicts the principle of generation of plasma in the PTAW process. A pilot arc is generated between the tungsten electrode acting as cathode and the constricting nozzle by means of potential difference applied between them. This pilot arc ionizes the gap between the substrate and the plasma nozzle resulting the generation of reliable high power plasma whose maximum instantaneous temperature can reach up to 20,000 ^{o}C. PTAW process offers many advantageous over GTAW for metallic material deposition. Some of the worth-mentioning advantages are (i) lesser HAZ; (ii) no risk of tungsten inclusion in the deposited material because tungsten electrode does not touch the molten pool as it is held within the constricting nozzle; (iii) enhanced life of the tungsten electrode; (iv) highly concentrated arc; (v) narrow and clean weld without any spatter marks; and (vi) higher precision.

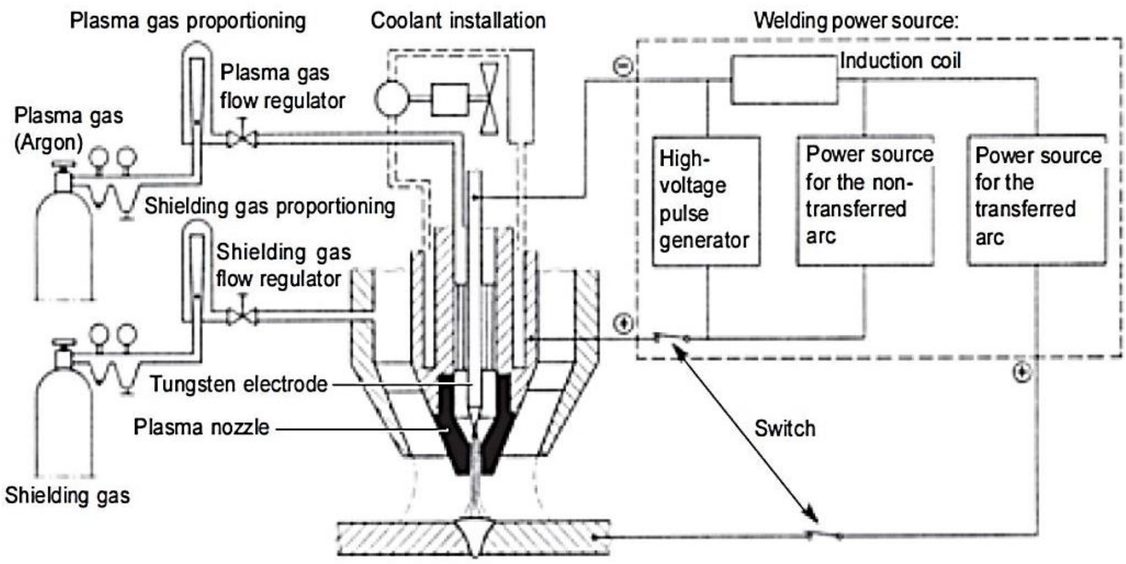

Fig. 1.5: Principle of generation of plasma in the PTAW process.

Both GTAW and PTAW use high current input generally in the range of 100 to 300 A. Consequently, these processes result in higher thermal distortion and generate adverse changes in the microstructure of the substrate. This problem can be solved either by developing micro-versions of these processes, preferably of PTAW due to its advantages over GTAW process. Use of very small amount of current will reduce the HAZ and thermal distortion of workpiece. With the advancement in digital power supply and process control, it is possible to develop micro-plasma transferred arc (µ-PTAW) process which can be operated at very low current of the order of 100 mA that too with finer control and high precision.

The principle of plasma generation in the µ-PTAW process is essentially same as that in the PTAW process. When pulsed power supply is used in the µ-PTAW process then it becomes pulsed µ-PTAW process, hereafter it is abbreviated as P-µPTAW. The P-µPTAW process can easily be programmed for different joining parameters to produce better quality weld joints. The weaving movement of the skilled welder can be done with an electronic ‘pulse’ that swings the join arc current from a peak to a background level, judiciously chosen to cause sufficient melting and allow enough time for the weld pool to coalesce into a solid joint. This process suits best for joining of miniature parts, very thin wires, rods, tubes and thin sheets. Current control up to 0.1 mA can provide precise micro-plasma arc to generate, target and concentrate the heat over very small area which gives smaller HAZ, low material distortion, deeper penetration, almost no porosity and inclusion and a joint having perfect appearance without any spatter marks. This process also offers improved steady arc direction, increased arc stability, greatly reduced the sensitivity to changes in arc length and is economical and, energy-efficient.

1.4.2.1 Advantages and Limitations

(1) Higher precision due to use of low current in the range of 0.1 to 20 A.

(2) Reduced heat input through built-in arc pulsation having pulse frequency in the range from 1 to 500 Hz.

(3) No arc-wander even at the lowest amperages.

(4) High pulse frequency arc starts and shuts off automatically.

(5) Short-duration of welding (can be as low as 0.002 seconds).

(6) In-built computer control makes it suitable for automatic welding.

(7) Use of robotic arm makes the joining process totally automatic.

(8) Highly accurate and repeatable welds with almost no HAZ and thermal distortion.

(9) Infrared and ultra-violet rays generated during the P-µPTAW are harmful to human being.

1.4.2.2 Process Parameters

It is important to understand various process parameters of P-µPTAW process and their respective functions during actual joining in order to under the process behavior and exercise better control. Fig. 1.6 illustrates various parameters of the P-µPTAW process with reference to a rectangular pulse and their effects on the joint quality are described below.

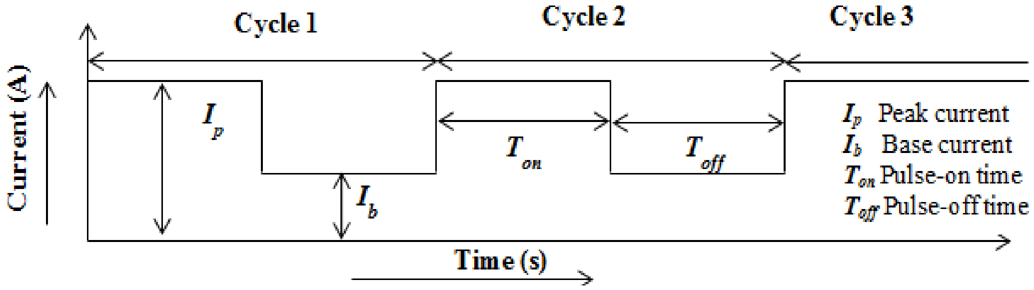

Fig. 1.6: Schematic representation of rectangular pulse in the P-µPTA joining process.

- **Pulse-on time** (T_{on}): Duration in which current attains its maximum value supplying the heat energy required to melt the base materials.
- **Pulse-off time** (T_{off}): Duration in which current has minimum sufficient to maintain the plasma arc between the nozzle and the base material. It is "cooling off" period between pulse-on times which allows solidification of the material melted during the pulse-on time.

- **Peak Current** (I_p): Peak current is the maximum value of pulsed current during pulse-on time and it must be sufficient enough to melt the material.
- **Base Current** (I_b): Base current is the minimum value of the pulsed current during pulse-off time and it must be sufficient enough to maintain the arc.
- **Pulse frequency** (f): Pulse frequency is the number of pulses per second. One pulse consists of one pulse-on and the adjacent pulse-off time. The pulse frequency depends on the required spot overlap.
- **Duty cycle** (τ): It is ratio of pulse-on time to sum of pulse-on time and pulse-off time and is expressed as percentage i.e. it indicate the % duration in which peak current is maintained. Its value is determined by the heat sensitivity of the material and the maximum current available from the power supply. Materials having higher thermal expansion may require a duty cycle on the peak current.
- **Plasma gas flow rate** (f_p): It is rate at which the plasma gas is supplied to form the pilot arc. Plasma gas helps to transfer the plasma power towards the joint materials and maintain a continuous directional flow of plasma towards the joint material.
- **Shield gas flow rate** (f_s): It is rate at which shield gas is supplied to protect the melt pool from atmospheric contamination. Lower values of the shield gas flow rate allow the atmospheric gases to react with the melt pool resulting in porous and oxidation of melt pool. Higher values result in the spread of molten pool generating dimple like impression over the top surface of join.
- **Torch travel speed** (V_t): It is the speed at which the joint material moves relative to the plasma nozzle. It decides the input energy per unit length. It is dependent on the flow rate of the material to be joined and the material thickness. The objective is to join the material as quickly as possible yielding a good quality joint. Torch travel speed is a predominant factor in defining the production output of a joining system.
- **Stand-off distance** (X): The distance from the electrode tip to the parts to be joined. It depends on the welding current, arc stability. It is important to keep the electrode at a fixed distance from the part surface with a sufficient gap to avoid stubbing out. It acts as a spark gap in P-µPTAW process. Higher stand-off distance may disconnect the plasma from the circuit. However, its lower values could restrain the formation of plasma with the highest possible energy for given values of the plasma power.

The most important parameters of the P-µPTAW are peak current (I_p), pulse frequency (f), duty cycle (τ) and torch travel speed (V_t). Various combination of this process parameter produces various quality of joint. A balanced combination of the plasma energy and torch travel speed is required for good quality of joint. Therefore, in the present work these parameters were selected as the variable parameters for different stages of experimentation to study their effects on the process performance of the P-µPTAW process. In addition of this, stand-off distance (X), plasma gas flow rate (f_p) and shield gas flow rate (f_s) also affect the process performance.

Chapter 2

Review of Past work and Research Objectives

2.1 Review of Past Work on Joining Thin Sheets

Following sections summarizes the review of the past work done using different welding processes namely GMAW, GTAW, LBW, EBW and PAW for joining thin sheets.

2.1.1 Past Work Using GMAW

Dean *et al.* (2005) studied joining of galvanized and zinc-aluminum thin sheets of thickness 1 mm using GMAW process. They investigated the relationship that exists between weld fusion, heat input and average cycle arcing current, and compared the performance of constant voltage control and current control welding techniques when welding coated steel sheets. It was observed that current control techniques produced more consistent weld penetration and fusion area. It was observed that weld spatter and any resulting coated surface damage can be significantly reduced using a current control technique.

Karadeniz *et al.* (2007) studied the effects of various process parameters of GMAW process on weld penetration in joining of 6842 steel sheets having 2.5 mm thickness. The welding current, arc voltage and welding speed were chosen as variable parameters. They observed that increasing current increased the depth of penetration. Arc voltage is another parameter that affects penetration. However, its effect is not as much as that of current. The effect of welding current on weld penetration is found to be approximately 2.5 times greater than that of arc voltage and welding speed. The optimum configuration found to be 105A, 24V, 80 cm/min to get optimum weld penetration and weld joint.

Kumar *et al.* (2009) investigated joining of Al 6082 alloy thin sheet of thickness 1 mm using vario wire 1 mm diameter in pulsed-GMAW (P-GMAW). Vario filler wire was passed between the rollers to get rectangular cross section (0.4 x1.2 mm). P-GMAW permitted a higher deposition rate, a lower energy input and fair gap-bridging capacity than the conventional GMAW process with a circular filler wire. Weld mismatch was found to increase with the increase in heat input primarily due to greater differential thermal expansion in HAZ and the base material. They observed that lap joints required more heat input than butt joints for the same thickness. Dilution in case of lap joints (10-25%) was less than that of butt joints (60-80%). Mechanical properties of the welds were found to be poor as the tensile strength of the 6082 alloy welds was around 150 MPa, and percent elongation was about 1.3% and it was primarily due to high porosity. They concluded that the porosity issue in DC P-GMAW welds needs further work to control it.

2.1.2 Past Work Using GTAW

Tarng and Yang (1998) studied joining of Al 1100 alloy sheets of thickness 1.6 mm by GTAW process. They investigated effect of various welding process parameters (arc gap, polarity ratio, welding speed, filler speed and welding current) on the weld bead geometry. The optimal weld bead geometry has a smaller-the-better quality characteristic for the front height, front width, back height, and back width of the weld bead. Through the analysis of variance, it was seen that welding speed, welding current, and polarity ratio are the important welding process parameters for the determination of the weld bead geometry. Subsequently, **Tarng *et al.*** (1999) developed an artificial neural network (ANN) model to construct the relationships between welding process parameters and weld pool geometry. Simulated annealing (SA) was applied to the ANN model for searching the process parameters for optimal weld pool geometry. Finally, the quality of aluminum welds based on the weld pool geometry was classified and verified by a fuzzy clustering technique.

Juang and Tarng (2002) reported on joining of SS304 thin sheets of 1.5 mm thickness and obtain optimal parameter for optimal weld pool geometry. Four input variables namely arc gap, flow rate, welding current and welding speed were selected to study weld pool geometry. Basically, the geometry of the weld pool has several quality characteristics (the front height, front width, back height and back width of the weld pool). Optimal weld pool geometry has smaller-the-better quality characteristics, i.e. the front height, front width, back height and back width of the weld pool. It was experimentally observed that weld pool geometry is improved by using GTAW process.

Balasubramanian *et al.* (2008a) investigated on joining of 1.6 mm thin sheets of Ti-6Al-4V alloy using pulsed-GTAW (PGTAW) process**.** They studies the effect of peak current, base current, pulse frequency, duty cycle to find out impact toughness and fusion zone grain size of the weldment. They observed that irrespective of changes in peak current and pulse frequency, the grain size has an inversely proportional relationship to impact toughness. The decrease in grain size and its effect to increase in toughness is attributed to the pulse nature of current. Microstructure of weldment revealed that the boundaries of primary α-grain were the preferential sites for crack nucleation and provide easy path for fracture propagation. Same authors (**Balasubramanian *et al.***, 2008b and 2010) reported on optimization of important pulse parameters (peak current, base current, pulse frequency, duty cycle) to maximize tensile properties (include ultimate tensile strength, yield strength and notch tensile strength) of the weld. Modified Taguchi method was used with success to identify the optimum parameters. Experimental results coupled with ANOVA results proved that pulse frequency has pronounced effect on the tensile properties. They also developed empirical relationships to predict the geometry of weld bead and shape relationships for the range of parameters used.

Kumar and Sundarrajan (2008) studied joining of Al 5456 alloy thin sheet of 2.14 mm thickness using PGTAW process. They investigated the influence of pulse parameters such as peak current, base current, welding speed, and pulse frequency on mechanical properties (ultimate tensile strength (UTS), yield strength, percent elongation and hardness). They developed a noble welding approach called roll planishing to improve the mechanical properties by passing the weld between two steel rollers. They observed 10-15% improvement in mechanical properties of the weld after roll planishing. This was due to relief or redistribution of internal stresses in the weld. Optimum welding parameters (Peak current 80A, Base current 40A, welding speed 230 mm/min, pulse frequency 4Hz) results increase in amount of Mg_2Al_3 precipitates and the metallographic analysis revealed a fine grain structure at the weld centre, which improved the mechanical properties.

Kumar and Datta (2012) reported the results of optimization of weld parameter on Ti-6-Al-4V of 2.5 mm thickness using PGTAW varying peak current, base current, pulse frequency, duty cycle and % of He in Ar-He mixture. Pulse current of 120 A, base current of 90 A, pulse frequency of 100 Hz, duty cycle of 70% and 20% of helium in Ar-He gas mixture produced weld with deep penetration.

Kumar *et al.* (2014) optimized PGTAW process parameters namely welding speed, current, voltage, stand-off distance to improve weld quality in terms of depth of penetration and width of weld for joint of SS 304 thin sheets of 1.6 mm thickness. Welding speed and current were found to be the most significant parameters. Weld strength was validated by tensile test and bend test. They observed that there is an improvement in tensile strength for optimal joint as compared to base material and bend test results in no opening or crack formation.

2.1.3 Past Work Using LBW

Farid *et al.* (2000) investigated the capabilities of photolytic iodine laser (PIL) for precision seam welding of SS316 0.1 mm thin sheets of 0.1 mm thickness. PIL offers much higher brightness than existing Nd:YAG and CO_2 lasers. The weld performance data of PIL laser were compared with Nd:YAG and CO_2 lasers. Benefits of PIL weld were narrow seam, extremely fine solidification cell structure, fully austenitic microstructure, and small HAZ. In contrast, the welds produced by Nd:YAG and CO_2 lasers exhibited wider seams, coarser solidification structures, duplex microstructures of austenite and ferrite, and larger HAZ due to slow cooling of the melt, and lateral heat diffusion. Despite the narrow seam, the PIL weld carried a high tensile load (92% that of base metal) and was harder than the base metal. Microstructural analysis revealed that PIL welds exhibited fully austenitic structures and were free from the hot cracking.

Klimpel *et al.* (2007) investigated the laser welding of 0.5 mm and 1.0 mm thick SS 321 sheets using a high power diode laser (HPDL). Welding of the steel sheets was carried out at different power of the laser beam and different welding speed. The width of butt joints of SS 321 sheets of 0.5 mm thick laser welded at optimal parameters is found below 2.0 mm and in case of butt joints of sheets 1.0mm thick, the width of joints is found below 2.4 mm. They conclude that the surfaces of laser welded SS joints are flat, smooth and with no undercuts and the height of the weld reinforcement is minimal. Also the optimal parameters produced weld of very high quality, without any internal imperfections and the structure and grain size of weld metal and HAZ is very narrow and the fusion zone is very regular.

Okamoto *et al*. (2008) studied joining of 0.25 mm thick sheets of (X5CrNi1810) stainless steel using two different modes of laser namely single-mode fiber laser and pulsed Nd:YAG laser at high speed with minimal distortion. Their studies revealed that narrow welding region obtained using a laser beam with a large focus diameter of 160 μm without pulse control, while a small focus diameter of 22 μm was found in general to provide good control of the welding state. A small focus diameter can result in an excellent welding seam from the start, even without pulse control. The penetration depth could be controlled by the energy density with a small focus diameter. It was observed that with a small focus diameter, the lap welding of 25μm thickness sheet could be successfully performed regardless of the presence of a small gap distance between two sheets.

Ventrella *et al*. (2010) used pulsed Nd:YAG laser welding process to join 0.1 mm thick AISI 316L foils. Joint with back penetration, no under fill and free from micro-cracks and porosity was obtained at an energy pulse of 1.75 J, with pulse frequency 39Hz and a 4 ms pulse duration. At this pulse energy the maximum ultimate tensile strength (UTS) was obtained. It was observed that the ultimate tensile strength (UTS) of the welded joints initially increased and then decreased as the pulse energy increased. A slight increase in the hardness in fusion zone and HAZ compared to those measured in the base metal was observed. This is related to the microstructural refinement in the fusion zone induced by rapid cooling.

Yilbas *et al.* (2010) used CO_2 laser for welding the mild steel sheets of thickness 2 mm under nitrogen assisted gas environment. Finite element method (FEM) was used to compute temperature and stress fields in the welding region. The residual stress developed in the welding region was measured using the X-Ray diffraction technique and the results were compared with the predictions with FEM method. Their study revealed that the stress attains high values in the cooling cycle after the solidification of the molten regions. This was because of repetitive absorption and dissipation of the laser energy in the molten zone which was generated in the surface region.

Mirakhorli *et al.* (2012) studied joining of duplex 2205 SS sheets having thickness of 2 mm using Nd:YAG pulsed laser. The microstructure of the weld metal was investigated at different travel speeds and pulse frequencies. In terms of the solidification pattern, the weld microstructure is shown to be composed of two distinct zones. At higher cooling rate, a higher percentage of ferrite is transformed to austenite. This is shown to be because with extreme cooling rates involved in pulsed laser welding, the ferrite-to-austenite transformation can be limited only to the grain boundaries.

2.1.4 Past Work Using EBW

Ananth *et al*. (2013) reported the joining of SS 304L to SS 446 tube of wall thickness 1.35 mm using EBW. Variables considered for welding were accelerating voltage, welding speed, beam current. They observed that beam current has the maximum effect (75.57%) on the penetration followed by accelerating voltage (17.26%) and weld speed (7.17%).The optimum parameter found to be 55kV as accelerating voltage, 9.33 mA as beam current and 0.8 m/min as weld speed. Microhardness of the weld bead lies in between that of parent metals indicating that parent metals are well diffused into the weld bead.

2.1.5 Past Work Using PAW

Zhang *et al.* (2000) used alternating current mode of PAW process to join LF6 aluminum alloy sheets of thickness 3 mm. They proposed ANN back propagation model to predict width of front melting, width of back melting, and weld reinforcement using welding current, arc voltage, welding speed, wire feed rate, and magnitude of ionizing gas flow rate.

Tseng *et al.* (2003) reported on weldability of 0.1 mm thick 304 SS sheets to produce an edge joint weld using micro-PAW and investigated the effects of the micro-PAW process parameters on the morphology and quality of SS edge joints. Welding experiments were carried out for various combinations of arc current, welding speed, arc length, shielding gas, and clamp distance. The experimental results indicated that the collimated shape of the low current plasma arc was mainly responsible for the low sensitivity of the weld morphology with variations in the nozzle stand-off distances. For stainless steel, mixture of 95% Ar and 5% H_2 produced high quality welds having very smooth surface. For high precision edge joint on 0.1mm thick SS sheets, a maximum gap of 0.05 mm is permitted.

Karimzahed *et al*. (2005) investigated on weldment of Ti6Al4V thin sheet of thickness 0.8 mm by micro-PAW process and investigated the effect of different current, welding speed and flow rates of shielding and plasma gas flow rate on grain growth and porosity distribution. They developed ANN model to predict grain size of fusion zone at different current and welding speeds. A critical energy input was observed, below which the fusion zone grain size remained almost constant and after this energy, width of fusion zone grains size increased continuously with an increase in energy input. Porosity occurs in welded metal by the addition of hydrogen.

Urena *et al.* (2007) investigated the optimum welding conditions (welding intensity and travel speed) for butt joint of 2205 duplex SS sheet of thickness 3mm for minimum net energy input using two different welding modes (i.e. the melt-in mode and, keyhole mode) of PAW. The influence of the welding parameters for each mode on the dimensions and shape of the welds and on their ferrite content was investigated. This study revealed that welds produced by keyhole PAW observed to have higher penetration/width ratios than welds produced in the melt-in mode. It also mentions that use of key-hole mode results lower input energies resulting in finer grain in fusion zone at higher temperature. They observed that by use of melt-in mode ferrite contents inside the fusion zone increases over 45% more than in the parent material while it is less than 20% when the keyhole mode is used.

Javidrad and Rahmati (2009) studied on joining of Ti-3Al-2.5V alloy sheets of thickness 0.8 mm and developed an experimental setup of PAW to produce specimens welded as butt joint under controlled welding parameters, such as voltage, current, travel speed, and shielding gas flow rate and studies their effects on tensile property, hardness and microstructure. The results of the tensile tests showed that the ultimate tensile strength of the most specimens is very near to that of the base material. Heat input of 99.75 J/mm gives most appropriate welding. Increase in hardness in the HAZ and fusion zone regions mainly occurs because of microstructure evolution due to heating and cooling process, poor edge preparation, and inclusion of atmospheric elements resulting from poor shielding of the weld pool.

Piccini and Svoboda (2012) studied on PAW of dual phase steel 700 of thickness 1.3 mm. The microstructure of these steels consists of a ferritic matrix with a variable fraction of a martensitic phase of high hardness. They analyzed the influence of heat input on the microstructural evolution and mechanical properties of dual phase steel welded joints. Nominal heat input in the range of 110 to 235 J/mm gave full penetration and defects-free joints. The best results were reached with 60 J/mm. The PAW process is shown to be an excellent choice for the welding of dual phase 700 steel because of its higher energy density, the HAZ becomes smaller without changing the mechanical properties. For low heat input values (55-80 J/mm), the HAZ size increases to a maximum, which is reached around 80 J/mm. Then, HAZ size decreases in the range of 80-100 J/mm. This could be related with the thermal pinch effect (related to the reduction of the arc diameter with the plasma gas flow). Therefore, increase in heat input with the increase in plasma gas flow, the energy density goes up, making the HAZ smaller.

Prasad *et al.* (2011a and 2011b) investigated the effect of welding speed on quality characteristics of weld of 0.25 mm thick SS 304 sheets (like weld pool geometry parameters, grain size, hardness and tensile properties and microstructure) joined by micro-PAW keeping pulse current constant. They observed over melting of base material at welding speed of 150 mm/min and improper fusion of the base material at welding speed of 300 mm/min. At the welding speed of around 260 mm/min optimum weld pool geometry was obtained. It was found that fusion zone grain size decreases up to 260 mm/min and thereafter it increases. Optimum hardness and ultimate tensile strength was also found at welding speed of 260 mm/min keeping other pulse parameters constant. Same authors (Prasad *et al.*, 2012c-e, 2013) presented a mathematical model (regression) to predict quality characteristics of SS 304 sheets. As peak current increases heat input increases leading to wider front and back widths and narrow front and back heights. Peak current also affects the grain size which signifies the hardness of weld joint. The weld joint obtained by micro-PAW is properly fused and is free from surface defects. The hardness values of the weld zone are comparatively better than the base material which indicates better strength of the weld joint. The grain size of base material in HAZ is around 45.4 μm and near to the fusion zone it is around 43.8 μm, which revealed that weld zone is stronger than base material.

Rao *et al.* (2012a-b) optimized the pulse parameter (peak current, back current, pulse frequency, pulse width) for joining of 0.25 mm thick Inconel 625 Sheets with an objective to optimize the ultimate tensile strength and grain size. Minimum grain size of 40.04 μm and maximum ultimate tensile strength of 857 MPa was obtained for the input parameters combination of peak current of 7 A, back current of 4 A, pulse frequency of 40 Hz and duty cycle 50%.

2.2 Identified Research Gaps

From the literature review it can be concluded that

- Limited work has been done on joining of thin sheets of stainless steel, aluminum, titanium etc.
- No work has been done on joining of thin sheet of 316L marine grade stainless steel having thickness less than 1 mm especially using micro-plasma arc welding process.
- No work has been done to understand the effect of pulse-on time and pulse-off time on variation of joint strength in pulse micro-plasma arc joining of SS thin sheets.
- There is lot of scope to understand plasma arc joining of different grades of SS using pulse current to obtain better joint characteristics.

2.3 Objectives of the Present Research Work

Present research work was undertaken with the following research objectives defined on the basis of the research gaps:

- To join thin sheets of SS 316L having thickness less than 1 mm and explore use of pulsed micro-plasma transferred arc (P-μPTA) joining process for the same.
- Detailed experimentation to know whether use of filler material is required in joining of very thin SS sheets, identify important process parameters of P-μPTA) joining process and bracket the range of identified variable process parameters
- To study the effects of pulse parameters and torch travel speed on strength and microstructure of the joint of thin SS sheets and reveal their importance.
- To optimize the important process parameters to maximize the joint strength.
- To find significant parameters using statistical analysis of the experimental results.
- To Study the changes in microstructure and microhardness of the joint.

Chapter 3

Planning and Details of the Experiments

This chapter presents the planning and details of experiments carried out in the present study. It describes the different sub-systems and the components of the experimental apparatus used in the present research work and planning of different experiments required for investigations on SS 316L thin sheet joining. It also presents the results of the preliminary experiments and characteristics of butt joint SS 316 L.

3.1 Experimental Apparatus

The experiments for the present work were conducted using the micro-plasma transferred arc wire deposition system developed by **Jhavar *et.al*** (2014) after suitable modification in wire feeder, support plate and clamps as per requirements of the thin sheet joining as shown Fig. 3.1. This experimental apparatus consists of following three major subsystems:

- Power source
- Manipulator system
- Wire Feeder

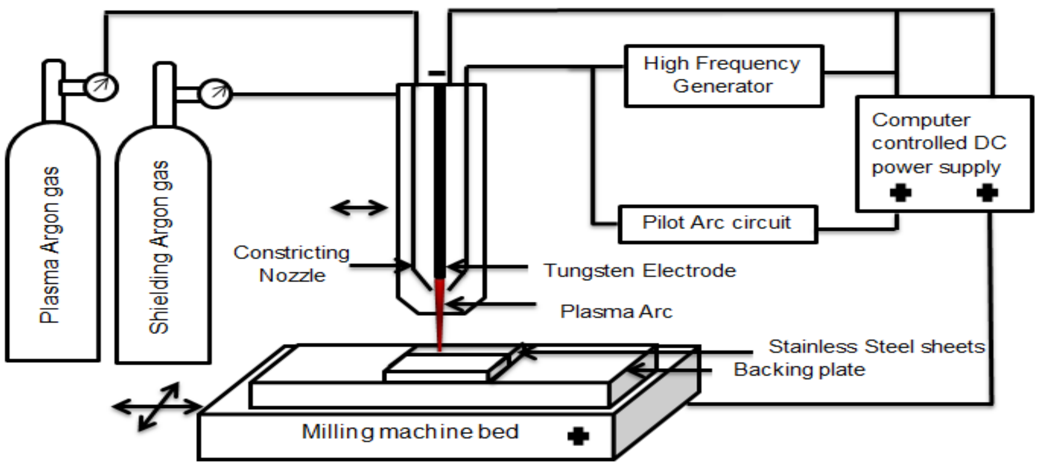

Fig. 3.1: Schematic diagram of experimental apparatus of P-µPTA joining process.

3.1.1 Power Source

A computer controlled micro-plasma joining power supply (model Dual arc 82HFP from pro fusion Inc. USA as depicted in Fig. 3.2), was used as power source in the experimental apparatus. The system offers dual process capability for micro-plasma joining and micro-TIG joining using the same power supply to provide flexibility for selecting the best process as per the requirement of an application. This micro-plasma control unit (MPCU) starts generating arc for current value between 0.1- 20A with weld capability for short duration of 0.01 seconds. Use of such a small value of current leads to many advantages such as; (i) gentle arc transfer, (ii) stable, stiffer arc with no arc wander, (iii) no high-frequency arc starting noise; (iv) extremely short duration of welds is possible for the applications of welding of wires, needles, and micro-components.

Fig. 3.2: Dual arc 82 HFP micro-plasma power source and controller.

The plasma torch *PlaTo-100* series with this power controller offers the best quality weld. Plato-100 series torch with copper nozzle of orifice diameter 500 micron gives stiff fine arc without wandering

3.1.2Manipulator System

A semi-automatic conventional horizontal milling machine (Model: HF1 from Bharat Fritz Werner Ltd.) as shown in Fig. 3.3 was used as manipulator (i) for mounting and moving the substrate in X-Y directions; and (ii) for controlling the torch travel speed and stand-off distance. This milling machine is a powerful precision knee-type milling machine ensuring vibration free and smooth movements. It has an automatic feed capability that makes the system suitable to control the torch travel speed. The machine has capacity to provide discrete transverse speed 40, 50, 63, 80,100, 125,200, 250, 315, 400, 500, 630, 800 mm/min in the automatic mode with a positional accuracy of 0.005 mm. A mounting plate was attached to the dog holes of the milling machine with the help of two long bolts and four nuts. The mounting plate serves the functions to hold the micro-plasma torch with the help of a mounting bracket. A 10 mm thick steel plate was used as backing plate with suitable clamps to hold the thin SS sheet firmly on the milling bed.

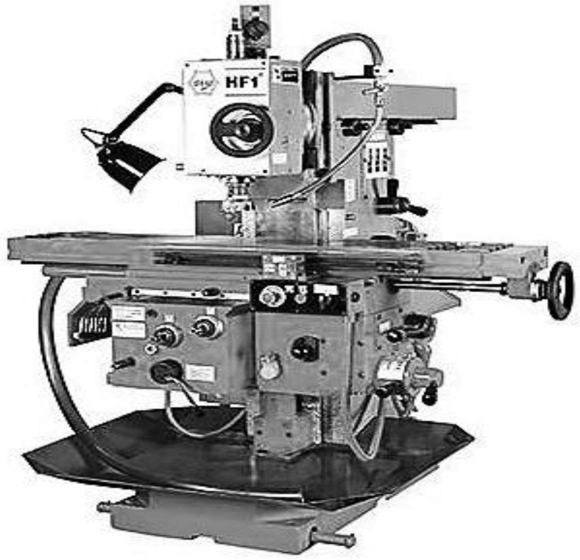

Fig. 3.3: Semi-automatic horizontal milling machine used as manipulator.

3.1.3 Wire Feeder

The wire feeding system was designed to be compact and having electronic speed control. Fig. 3.4 shows the design of wire feeder with electronic speed controller. A wire feed roll was attached to the wire feeding system to provide continues feed of wire. Wire feeding system consists of driver pulley and driven pulley. The driver pulleys were provided with a variable speed motor connected electronically to control such that it can provide sufficient amount of the filler wire at the feed rates in the range of 60-600 mm/sec.

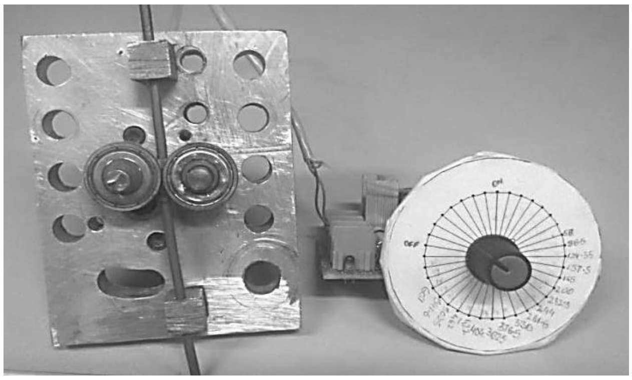

Fig. 3.4: Design of wire feeder with electronic speed controller.

3.2 Selection of Material

In the present study, thin sheets of SS 316L having thickness of 0.4 mm and filler wire of 0.274 mm diameter of the same material were chosen. SS316L is an austenitic stainless steel containing chromium, nickel and molybdenum. Table 3.1 presents its chemical composition. It is known as marine grade steel and is best suited for corrosion resistance applications. Chromium provides resistance to oxidation, improving hardenability and strength**.** Nickel increase corrosion and heat resistant in steels and molybdenum increases resistance to pitting corrosion especially against chlorides and sulphur. Stainless steel material was tested and verified as SS316L alloy in the Quality Test Laboratory, Mumbai under T/C No: Z/10688

Table 3.1: Chemical composition of SS 316L.

% (w/w)	C%	Si%	Mn%	P%	S%	Cr%	Mo%	Ni%
Elements	0.026	0.370	1.050	0.030	0.012	16.700	2.0900	10.1500

3.3Plan of Experimentation

Several experiments were planned and performed to determine the feasibility of joint. Here different combinations of the joining parameter were used. All the experiments are divided into two parts: Preliminary experiments to judge the feasibility of joint (3.2.1) and, main experiments (3.2.2) to determine the mechanical properties and microstructure of the joint.

3.3.1 Preliminary Experiments

Preliminary experiments consisted of various experimental approaches taken to get a feasible parameter determination for joint with good back penetration.

3.3.1.1 Experiments Using Continuous Power Supply

To study the effect of continuous power supply, the plasma beam is directed to a single SS sheet using value of direct current in decreasing order (i.e. 10, 9, 8, 7, 6, 5, 4, 3, 2, 1, 0.9A) at with torch travel speed of 250 mm/min. It was found that DC produces more heat which result in burn through of SS sheets even at value of DC of 0.9 A as shown in Fig. 3.5. Based on these results, decision was taken to pulse power for joining the thin SS sheets.

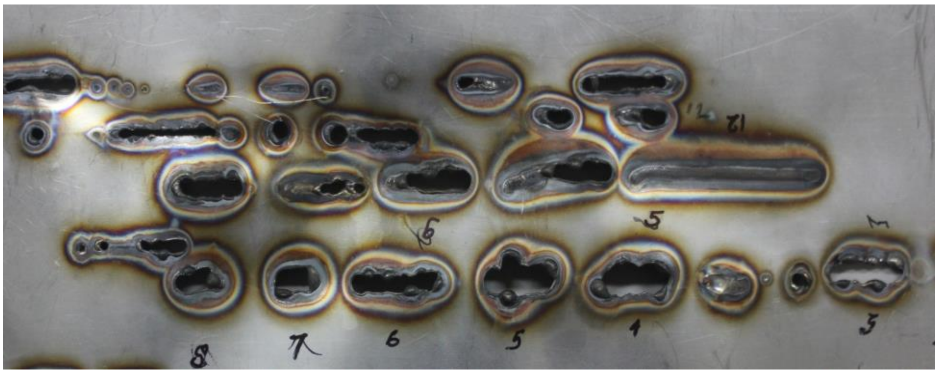

Fig. 3.5: Experiments with Continuous power supply on single SS sheet.

3.3.1.2 Experiments Using Filler Wire

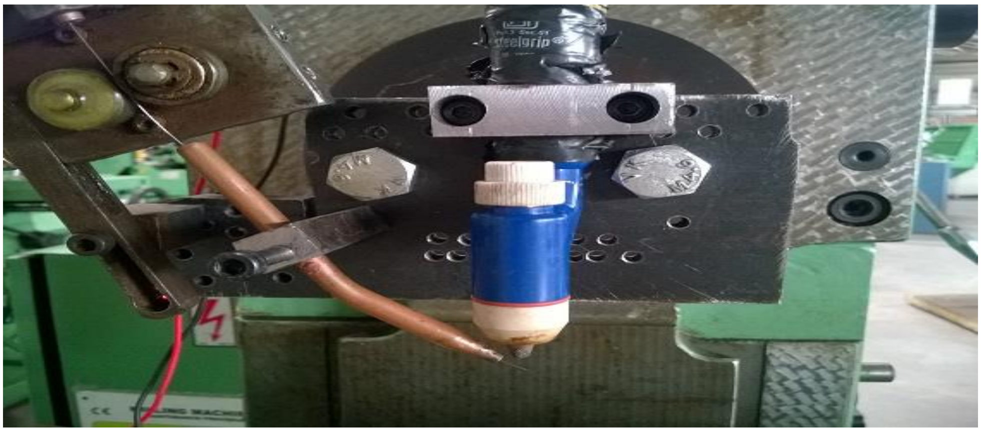

Fig. 3.6*:* *Plato100* plasma torch with wire feeder.

In the present work, experiments were conducted on homogeneous joining of 0.4 mm thin stainless steel sheets using wire of same material and having 0.274 mm diameter. These experiments could not join the thin SS sheets successfully and considerable difficulties were faced in feeding the small diameter wire and to align it with the edge to be joined. Therefore, it was decided to use autogeneous joining (i.e. no filler material) for further experiments. This decision is in confirmation with the dependence of filler material requirement and edge preparation on the thickness of the sheet for different joining processes as illustrated in Fig 3.7.

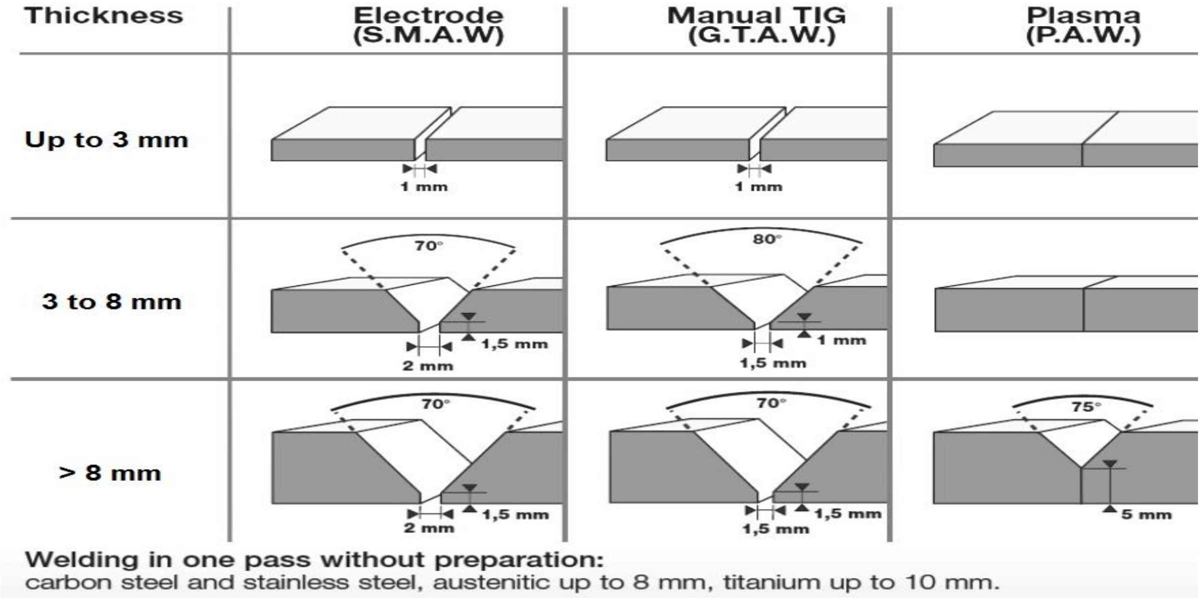

Fig. 3.7: Dependence of filler material requirement and edge preparation on sheet thickness for different joining processes.

3.3.1.3 Pilot Experiments (Stage-1)

Based on the obtained experiments results while using continuous power supply and filler wire, pilot experiments were planned on autogeneous joining of thin SS sheets suing pulsed current in μ-PTA joining process to determine the feasible ranges of the pulse parameters and torch travel speed to obtain a fused joint with sufficient back penetration. In these experiments ends of the sheet were spot welded, and clamped with adequate pressure to firmly hold the sheets without any mismatch in the edge. The component edges are accurately machined so that the two faces are in perfect contact along the entire length of the joint. Table 3.2 presents the ranges of the parameters used in the stage-1 of pilot experiments and the number of experiments performed for each variable parameter. In all these 54 pilot experiments (stage-1) asbestos sheet of dimensions 40 mm x 10 mm was used as the backing plate. Table 3.3 presents experimental observations for the stage-1 of pilot experiments.

Table 3.2: Ranges of the variable parameters and values of the constant parameters pilot (stage-1) experiments.

Parameter	Unit	Range available on MPCU	Selected range of the parameter	No. of Experiment
Peak current	A	0.1-20	0.5- 5.0	18
Pulse frequency	Hz	1-500	10 – 40	12
Duty cycle	%	1-99	30 – 60	12
Torch travel speed	mm/min	40-800	125- 315	12
Total no. of experiments: 54				
Constant parameters: Plasma gas(flow rate): Argon(0.2 lpm); Shielding gas(flow rate): Argon (5 lpm); Base current: 0.2A; Stand-off distance: 3 mm; Nozzle orifice: 0.5mm				

Table 3.3: Experimental observations for pilot (stage-1) experiments.

(A) Experiments 1-18 describes the effect of peak current on welded joint at pulse frequency 20 Hz , duty cycle 50 % and torch travel speed 200 mm/min.

Exp. No.	Peak current	Top View	Observations
1	0.5	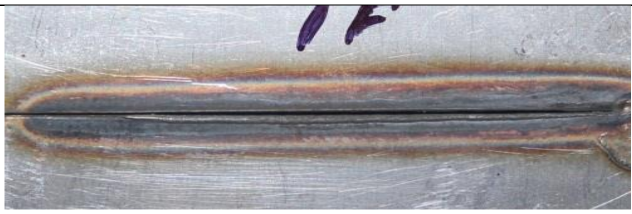	No Fusion*
2	0.7	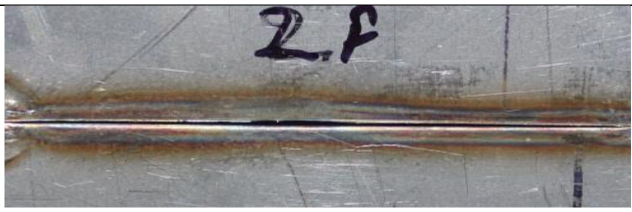	No Fusion*
3	1.0		No Fusion*
4	1.3		No Fusion*
5	1.7		No Fusion*
6	2.0		No Fusion*
7	2.2		No Fusion*

8	2.5		No Fusion*
9	2.7		No Fusion*
10	3.0	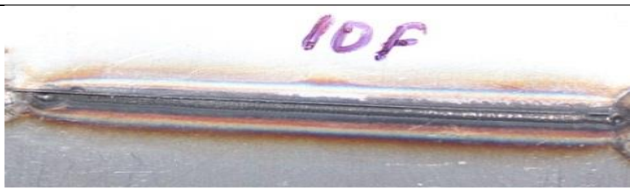	Fusion*
11	3.2		Fusion*
12	3.5		Fusion*
13	3.8		Fusion*
14	3.8	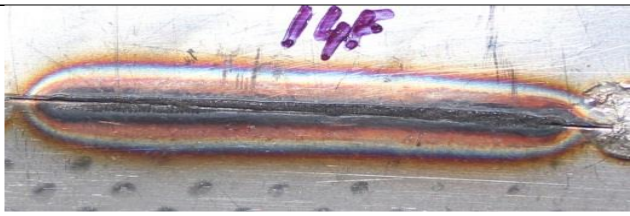	Fusion*
15	4.0	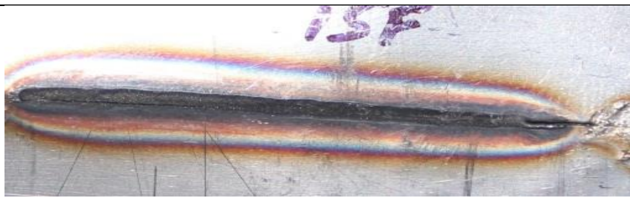	Fusion*

16	4.3		Fusion*
17	4.6	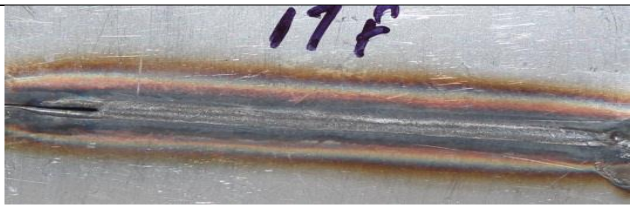	Fusion*
18	5.0	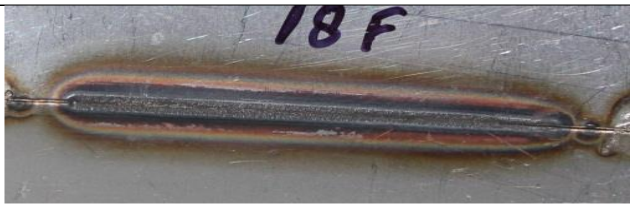	Fusion*

(B) Experiments 19-30 describe the effect of pulse frequency at different peak currents on welded joint, at constant values of duty Cycle 50 % and torch travel speed 200 mm/min

Exp. No.	f	I_p	Top View	Observations
19	10	3	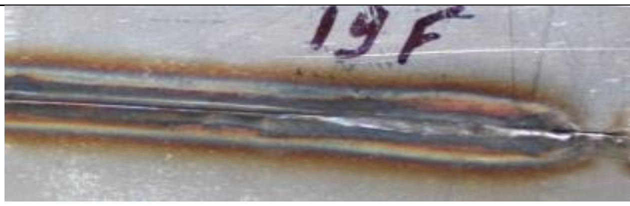	Fusion*
20	20	3		Fusion*
21	30	3		Fusion*
22	40	3		Fusion*

23	10	3.5	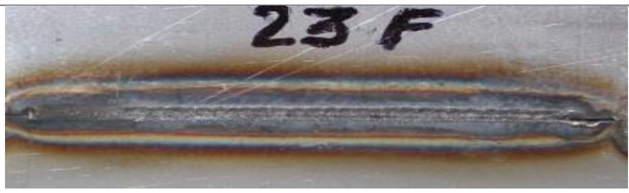	Fusion*
24	20	3.5		Fusion*
25	30	3.5		Fusion*
26	40	3.5	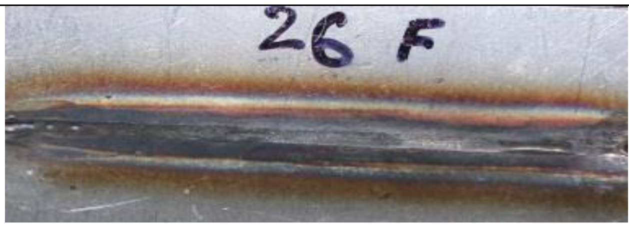	Fusion*
27	10	4	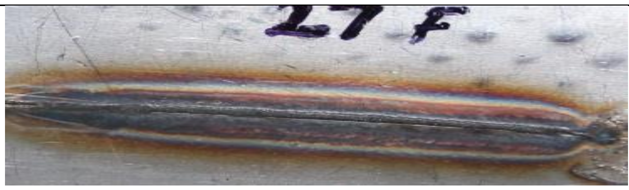	Fusion*
28	20	4		Fusion*
29	30	4	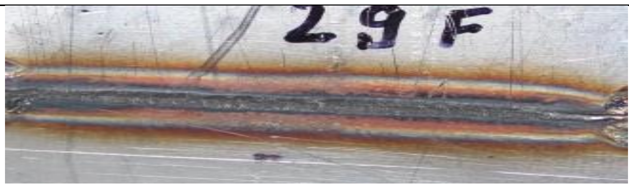	Fusion*
30	40	4		Fusion*

(C) Experiments 31-42 describe the effect of duty cycle at different peak currents on welded joint, at constant values of pulse frequency 20 Hz and torch travel speed 200 mm/min

Exp. No.	τ	I_p	Top view	Observations
31	30	3	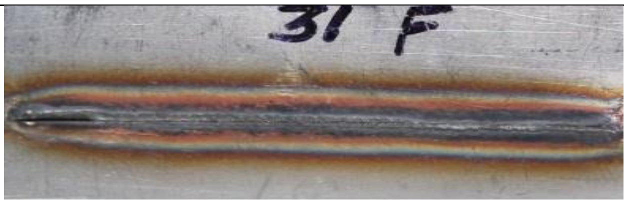	Fusion*
32	40	3	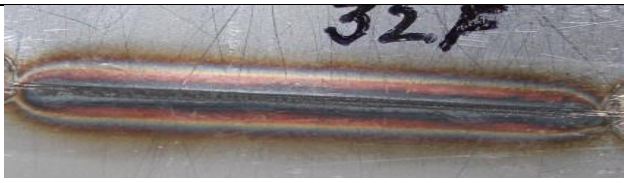	Fusion*
33	50	3	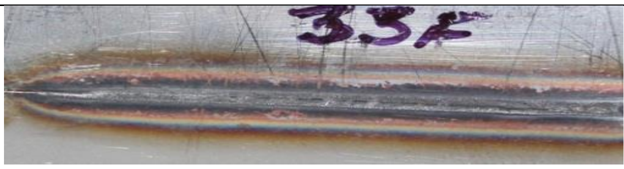	Fusion*
34	60	3		Fusion*
35	30	3.5		Fusion*
36	40	3.5	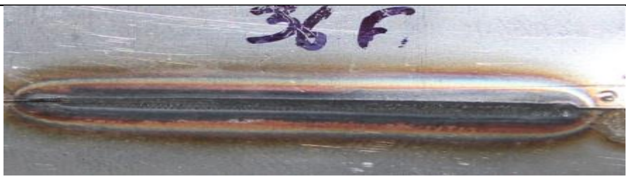	Fusion*
37	50	3.5	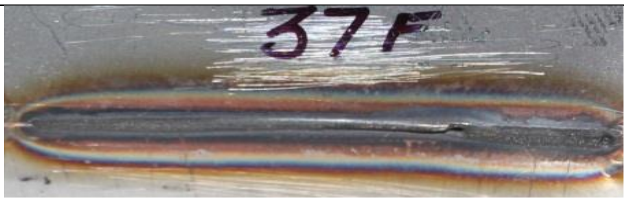	Fusion*
38	60	3.5		Fusion*

39	30	4	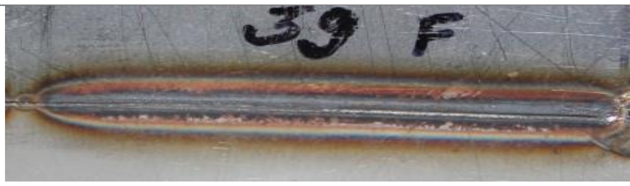	Fusion*
40	40	4		Fusion*
41	50	4		Fusion*
42	60	4	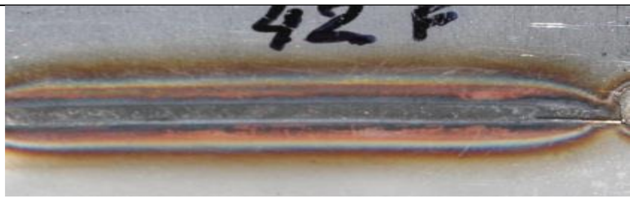	Fusion*

(D) Experiments 43-54 describe the effect of torch travel speed at different peak currents on welded joint, at constant values of pulse frequency 20 Hz and duty cycle 50%

Exp. No.	V_t	I_p	Top view	Observations
43	125	3	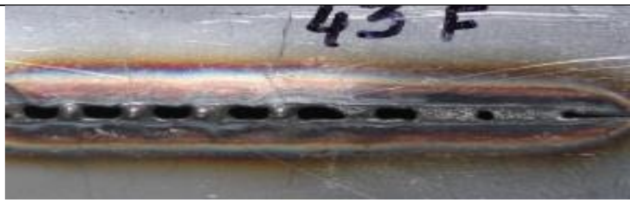	Burn through
44	200	3		Fusion*
45	250	3		Fusion*
46	315	3		No Fusion

47	125	3.5	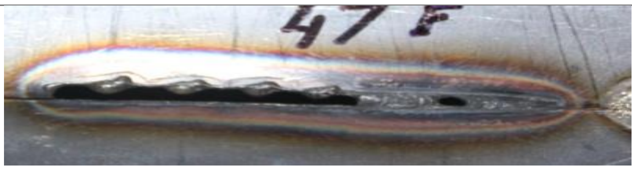	Burn through
48	200	3.5		Fusion*
49	250	3.5		Fusion*
50	315	3.5		No Fusion
51	125	4		Burn through
52	200	4		Fusion*
53	250	4	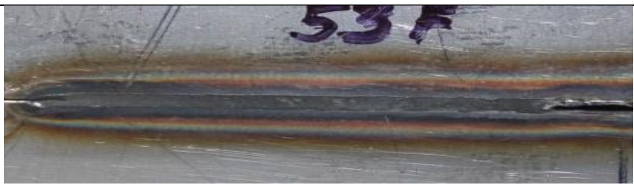	Fusion*
54	315	4		No Fusion

**In all fused joint the back side of bead appeared black in color with insufficient penetration. This may be due to use of asbestos as a backing plate, which acts as insulator and resist the sheet to cool down, resulted in improper bead color and appearances.*

From the experimental results of Table 3.3, following observations can be made:

(i) The values of peak current below 2.5A did not produce sufficient heat for joining (refer experiment number 1 to 9).

(ii) In all the experiments from number 10 to 42, a fused joint was observed for different combinations of experimental parameters.

(iii) A torch travel speed of 125 mm/min resulted in burn through due to high amount of localized heat input. A torch travel speed of 315 mm/min resulted in unfused joint due to insufficient time for melting the sheets.

From the above observations, it was concluded that peak current within the range 2.7 to 5.0 A, frequency 10 to 40 Hz, duty cycle 30 to 60% and torch travel speed 200 and 250 mm/min are found to produce a fused joint.

(iv) All experiments from 1 to 54, the back side of joint bead appearance was observed to be blackish with insufficient penetration. Appearance of black bead on the back side was due to use of asbestos as backing plate. Asbestos acts as insulator and resist the sheet to cool down, resulted in blackish back side bead appearances. Insufficient penetration was due to use of low base current of 0.2 A.

Observation (iv) led to change the material of backing plate from asbestos to stainless steel and increase the base current to 1A. To verify the changes that may occur with use of steel backing plate and base current value of 1A led to good fused joint with back penetration, 24 more pilot experiments were done and they are referred as pilot experiments (stage-2).

3.3.1.4 Pilot Experiments (Stage-2)

To verify the ranges of parameters identified during stage-1 of pilot experiments, further pilot experiments (stage-2) were performed by using 1 A base current and backing plate of steel. From the available ranges of the peak current, frequency, duty cycle and torch travel speed, a total of 24 experiments are decided to perform using one factor at a time approach. Table 3.4 lists the available and selected range of the parameters along with number of experiments done for each parameter. Table 3.5 lists experimental observations for stage-2 of the pilot experiments.

Table 3.4 Ranges of the variable parameters and values of the constant parameters pilot (stage-2) experiments.

Parameter (Unit)	Range available on MPCU	Selected range of the parameter	Mean value of parameters	Least count	Increment	No. of Exp.
Peak current (A)	0.1 – 20	1.5-6.0	3.5	0.1	0.5	10
Frequency (Hz)	1-500	10-60	35	01	10	6
Duty Cycle (%)	1-99	20-80	50	01	10	7
Torch travel speed (mm/min)	40-800	125,200,250,315 ,400	(262.5)250	---		05
Base current (A)	5 – 90% I_p	1	Total number of experiments 24			
Backing plate: Stainless Steel plate of dimensions 250 mm x 100 mm						
Constant parameters: Plasma gas(flow rate): Argon(0.2 lpm); Shielding gas(flow rate): Argon (5 lpm); Base current: 0.2A; Stand-off distance: 3 mm; Nozzle orifice: 0.5mm						

Table 3.5: Experimental observations for pilot (stage-2) experiments.

(A) Runs 1-10 describe the effect of peak current at constant values of pulse frequency 35 Hz , duty cycle 50% and torch travel speed 250 mm/min.			
Exp. No	I_p	Top View	Observations
1	1.5	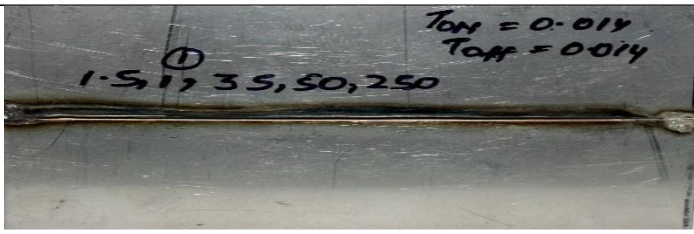	No Fusion
2	2.0	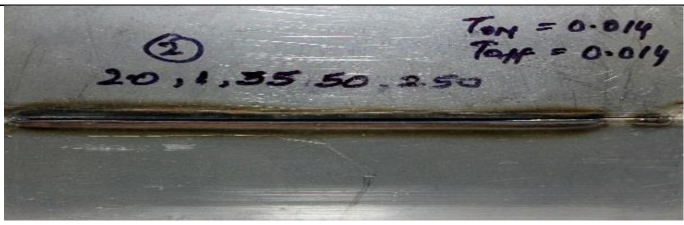	No Fusion
3	2.5	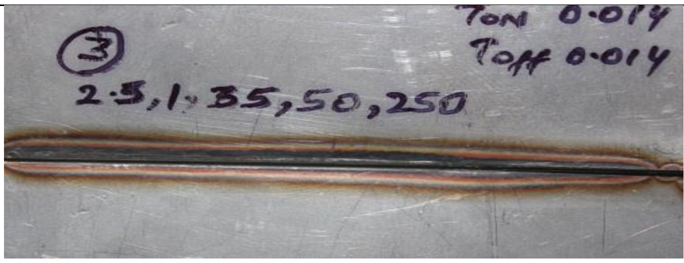	No Fusion

4	3.0		Fusion with no back penetration
5	3.5		Fusion
6	4.0		Fusion
7	4.5		Fusion
8	5.0		Fusion
9	5.5	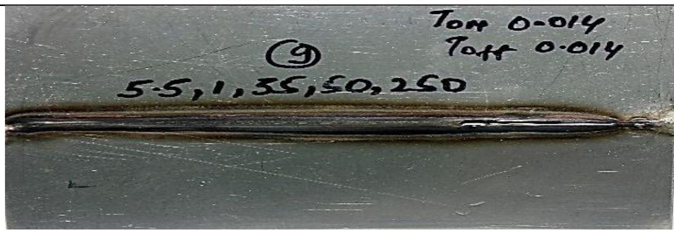	Fusion
10	6.0		Burn through

(B) Runs 11-16 describe the effect of frequency at constant values of peak current 3.5 A, duty cycle 50% and torch travel speed 250 mm/min			
Exp. No	*f*	Top View	Observations
11	10		Fusion with back penetration
12	20	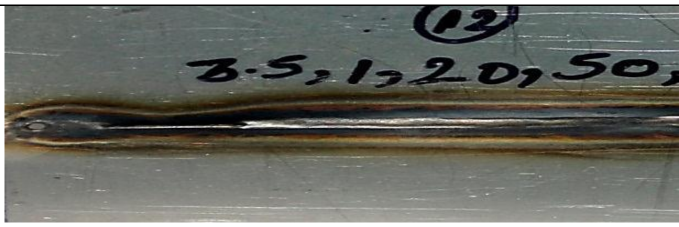	Fusion with back penetration
13	30		Fusion with back penetration
14	40		Fusion with small back penetration
15	50		No Fusion
16	60	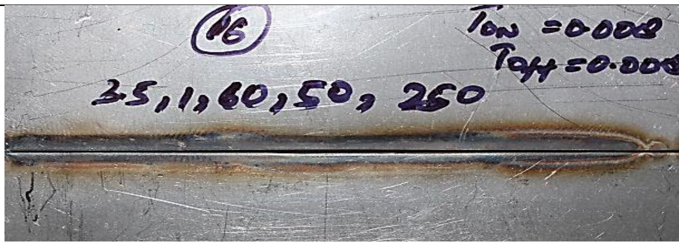	No Fusion

(C) Runs 17-23 describe the effect of duty cycle at constant values of peak current 3.5 A, frequency 35 Hz and torch travel speed 250 mm/min

Exp. No.	τ	Top View	Observations
17	20	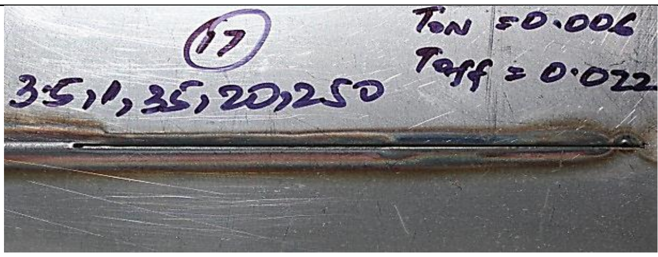	No Fusion
18	30	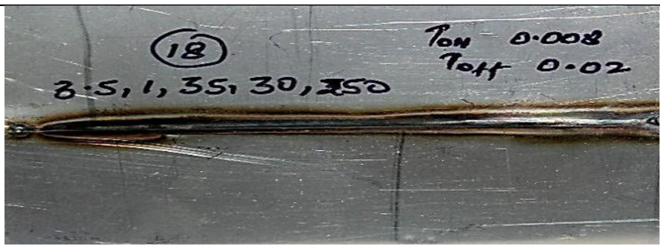	Fusion with no back penetration
19	40	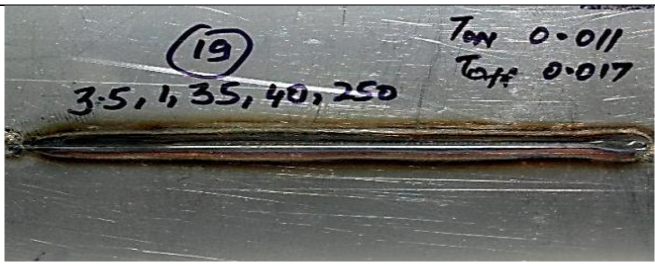	Fusion with no back penetration
20	50	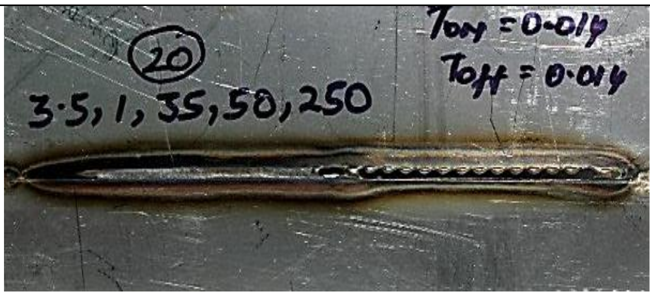	Joint with back penetration *Small cut due to misalignment
21	60		Fusion with back-penetration *small burn through Due to misalignment

22	70		Fusion with back penetration *small burn through due to misalignment
23	80		Burn through

(D) Experiments 24-28 describe the effect of torch travel speed at constant values of peak current 3.5 A, duty cycle 50% and torch travel speed 250 mm/min

Exp. No.	V_t	Top View	Observations
24	125		Burn through
25	200		Fusion with back penetration
26	250	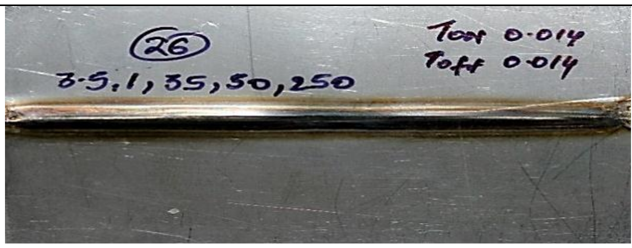	Fusion with back penetration
27	315		No Fusion

28	400	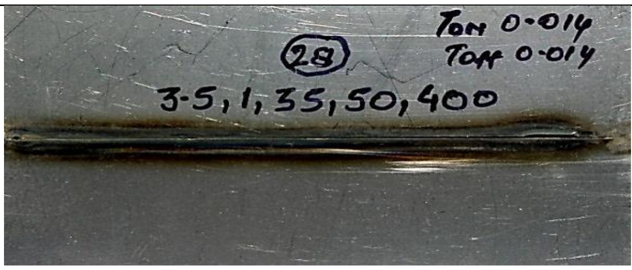	No Fusion

From the experimental results of table 3.5, following observations can be made:

(i) The values of peak current below 2.5A resulted in unfused joint [refer experimental number 1 to 4]. This indicates that peak current up to 2.5 A could not produce sufficient heat required for the melting and fusion. These observations reconfirm the findings of pilot (stage-1) experiments. Peak current of 3A resulted fusion joint with insufficient back side penetration.

(ii) Peak current in range of 3.5 to 5.5A yielded fused joint with back penetration [refer experiment number 5 to 9]. Peak current of 6A produced burn through due to excessive heat input in the fusion zone [experiment number 10].

(iii) Pulse frequency in range of 10 to 30 Hz resulted in fused joint with back penetration [refer experiment number 11 to 13] whereas 40 Hz resulted in fusion joint with small back side penetration [refer experiment number 14]

(iv) Pulse frequency in range of 50 to 60 Hz produces unfused joint [experiment number 15 and 16].

(v) Duty cycle 20% yield unfused joint [experiment no. 17] whereas 30 to 40% duty cycle produces fusion joint with no back side penetration [experiment number 18 and 19]

(vi) Duty cycle in range of 50 to 70% resulted in fused joint with back side penetration [refer experiment number 20 to 22] and 80% duty cycle yielded burn through [see experiment no. 23]

(vii) Torch travel speed of 125 mm/min produced burn through due to high localized heat input at slower torch travel speed [experiment no. 24]. Whereas 200 and 250 mm/min torch travel speed yielded proper melt and fused joint [refer experiment number 25 and 26]. Torch travel speed 315 and 400 mm/min gave unfused joint due to insufficient melting time [experiment no. 27 and 28]. This observations reconfirm the findings of pilot (stage-1) experiments.

From the above observations, it was concluded that peak current 3.5 to 5.5 A, frequency 10 to 30 Hz, duty cycle 50 to 70 % and torch travel speed 200 and 250 mm/min are found to be suitable for melting and form a fusion joint with back side penetration. These ranges of the parameters were selected for use in the main experiments.

3.3.2 Main Experiments

Based on the results of the pilot experiments, ranges of four parameters were determined for the main experiments to obtain a fused joint of thin SS sheets with sufficient back penetration. The main experiments were designed using full factorial design of experiment approach. In these experiments, the joint was evaluated by measuring its ultimate tensile strength and microhardness. Additionally microstructure of joint is also determined. Table 3.6 lists the variable and constant parameters used in the main experiments.

Table 3.6: Details of variable and constant parameters used in the main experiments.

Parameter name (unit)	Range	Levels				
		1	2	3	4	5
Peak current (A)	3.5 - 5.5	3.5	4.5	5.5		
Pulse frequency (Hz)	10 - 30	10	20	30		
Duty cycle (%)	50 - 70	50	60	70		
Pulse-on time (s)	0.02-0.07	0.02	0.03	0.05	0.06	0.07
Pulse-off time (s)	0.013-0.05	0.013	0.02	0.05	0.04	0.03
Torch travel speed (mm/min)	200- 250	200	250			
Constant parameters: Plasma gas (flow rate): Argon (0.2 lpm); Shielding gas (flow rate): Argon (5 lpm); Base current: 1A; Stand-off distance: 3 mm						

In P-μPTA joining process, pulse-on time and pulse-off time are the important parameters. Pulse-on time governs the time required for melting whereas pulse-off time governs the time required for solidification. Both times are influenced by pulse frequency and duty cycle. Pulse-on time and pulse-off time are calculated through equations 1a to 1d. These calculated values are included in table 3.6.

$$Pulse\ frequecy\ (f) = \frac{1}{T_{on} + T_{off}} \ldots\ldots (1a) \qquad Duty\ cycle\ (\tau) = \frac{T_{on}}{T_{on} + T_{off}} \ldots\ldots (1b)$$

$$Pulse-on\ time\ (T_{on}) = \frac{\tau}{100\,f} \ldots. (1c) \quad Pulse-off\ time\ (T_{off}) = \frac{1}{f}\left(1 - \frac{\tau}{100}\right) \ldots (1d)$$

Out of nine combinations of duty cycle and pulse frequency, only five combinations (i.e. 30 Hz and 60%; 20 Hz and 60%; 10 Hz and 50%; 10 Hz and 60%; and 10 Hz and 70%) were chosen giving values of T_{on} and T_{off} as 0.02 and 0.013 s; 0.03 and 0.02 s; 0.05 and 0.05 s; 0.06 and 0.04 s; and 0.07 and 0.03 s. This was done to reduce the large number of experimentation and ease of experimentation. Full factorial design was used varying pulse-on time and pulse-off time at five levels, peak current at three levels and torch travel speed at two levels. Thus, total thirty main experiments were conducted.

3.4 Evaluation of the Joint

The joint of the SS thin sheet was evaluated by measuring its tensile strength for all the main experiments whereas micro-hardness and microstructure was evaluated for the optimal joint only.

3.4.1 Tensile strength

Specimen for tensile strength test was prepared according to ASTM E8 standard and was cut by wire electric discharge machining (WEDM) process so that the joint is in the middle of the specimen. The geometry of specimen used for tensile testing is shown in Fig. 3.8.

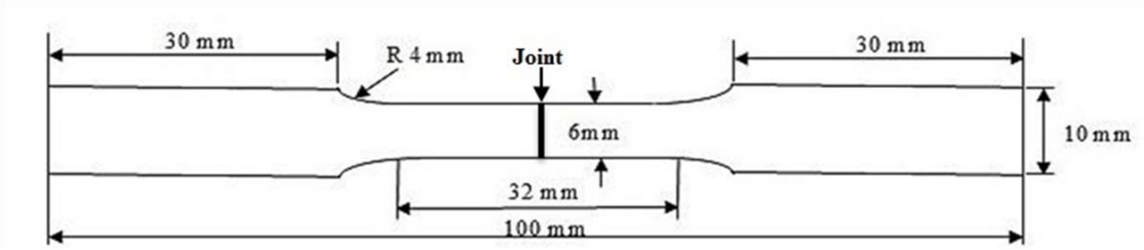

Fig. 3.8: Configuration of specimen for determining tensile strength of the joint.

Tensile strength was determined using a universal testing machine (model ***Tinius Olsen H50KL***, ***USA***) with cross-head speed of 1 mm/min. The joint strength was considered as ultimate tensile strength of specimen. Ultimate tensile strength of the sheet material was found to be 582 MPa. All the specimens were found to fail from the joint position.

3.4.2 Microstructure

Examination of microstructure of optimal joint is important to understand the phase transformation across different zone (Base material, Fusion Zone, HAZ). In order to characterize the microstructure of optimal joint, a sample (dimension 10 mm x 6 mm) was sectioned in transverse direction using WEDM process. Sectioned samples were mounted using cold setting resin to facilitate holding the samples during polishing. Sample were then polished on the polishing machine using polishing papers of different grades, starting from 220, 400, 600, 800, 1000, 1500, 2000 and 2500. After this selvet cloth was used for polishing with diamond paste of 1 µm to get a mirror finish. These polished samples were then cleaned with isopropanol to remove the any dirt or diamond paste adhered to it. Samples were then etched using chemical reagent having composition of 2g $CuCl_2$, 40 mL HCl, 40 ml 96% ethanol and 40 ml water for less than 30 seconds. The etched samples were then observed under the inverted optical microscope. Results of microstructure of optimal joint were analyzed and reported in next chapter.

3.4.3 Microhardness

As indicated by the Hall-Petch relationship, hardness is a function of grain size (Liu. *et al.*, 2003) and can be given by

$$H = H_o + kd^{-\frac{1}{2}}$$

Where, H is hardness, d is grain size, and H_o, k are constants. Hardness varies with the reciprocal square root of grain size i.e. the region in which grain size decreases results increase in hardness. The microhardness was measured in longitudinal direction (Top surface) to find the hardness variation across the joint and find significance of HAZ and hardness variation using Vickers micro-hardness machine (*UHL VMH-002* from Walter UHL GmbH, Germany). A load of 200 g was applied for the duration of 10 seconds. Result of Vickers microhardness for optimal joint were analyzed and reported in next chapter.

Chapter 4

Results and Discussion

This chapter presents results of the main experiments (Table 4.1), their analysis, variation of joint strength with different pulse parameters and torch travel speed and identification of their optimum values for maximum joint strength, results of analysis of variance (ANOVA) to determine the significant parameter and evaluation of microstructure and microhardness of the optimal joint.

Table 4.1: Values of input parameters and joint strength for different main experiments.

Exp. No	Peak current 'I_p'(A)	Torch travel speed 'V_t' (mm/min)	Pulse frequency 'f' (Hz)	Duty cycle 'τ' (%)	Pulse-on time 'T_{on}' (s)	Pulse-off time 'T_{off}' (s)	Ultimate tensile strength of joint (MPa)
1	3.5	200	30	60	0.02	0.013	440
2	3.5	200	20	60	0.03	0.02	494
3	3.5	200	10	50	0.05	0.05	523
4	3.5	200	10	60	0.06	0.04	460
5	3.5	200	10	70	0.07	0.03	333
6	4.5	200	30	60	0.02	0.013	431
7	4.5	200	20	60	0.03	0.02	467
8	4.5	200	10	50	0.05	0.05	512
9	4.5	200	10	60	0.06	0.04	455
10	4.5	200	10	70	0.07	0.03	297
11	5.5	200	30	60	0.02	0.013	416
12	5.5	200	20	60	0.03	0.02	450
13	5.5	200	10	50	0.05	0.05	490
14	5.5	200	10	60	0.06	0.04	435
15	5.5	200	10	70	0.07	0.03	361
16	3.5	250	30	60	0.02	0.013	492
17	3.5	250	20	60	0.03	0.02	505
18	3.5	250	10	50	0.05	0.05	553
19	3.5	250	10	60	0.06	0.04	499
20	3.5	250	10	70	0.07	0.03	392
21	4.5	250	30	60	0.02	0.013	465
22	4.5	250	20	60	0.03	0.02	509
23	4.5	250	10	50	0.05	0.05	517
24	4.5	250	10	60	0.06	0.04	491
25	4.5	250	10	70	0.07	0.03	359
26	5.5	250	30	60	0.02	0.013	453
27	5.5	250	20	60	0.03	0.02	497
28	5.5	250	10	50	0.05	0.05	514
29	5.5	250	10	60	0.06	0.04	470
30	5.5	250	10	70	0.07	0.03	398

4.1 Variation of Joint Strength

Fig. 4.1 (a) and (b) show the variation of joint strength with pulse-on time at different peak currents for constant torch travel speed of 200 mm/min and 250 mm/min respectively. The corresponding pulse-off time is shown on the top of figure respectively. It can be seen in both the figures that the joint strength increases with increase in pulse-on time, reaches maximum value at 0.05 s and thereafter decreases. This observation is valid for all the values of peak current at different torch speeds.

Consequently, an optimum combination of pulse-on and pulse-off times and correspondingly combination of duty cycle and pulse frequency exists for maximum joint strength for all three values of the peak current and two values of the torch travel speed. In the present case, the optimum values obtained are 0.05 s for both T_{on} and T_{off} corresponding to duty cycle equal to 50 % at 20 Hz pulse frequency. This can be explained by the fact that to yield good strength and quality of the joint, an optimum balance should be there between the time available for melting and fusing of the sheet material (i.e. T_{on}) and the time available for solidification of the molten and fused material in the joint (i.e. T_{off}). Lower value of T_{on} will result in insufficient melting whereas very high value of T_{on} will result in burn through. Therefore, an optimum values of T_{on} and T_{off} exist and correspondingly optimum combination of duty cycle and pulse frequency.

It can also be observed from Fig. 4.1 that for each combination of T_{on} and T_{off} (i) the joint strength increases with decrease in peak current except for T_{on} equal to 0.07 at both the values of the torch travel speed; and (ii) the joint strength increase with increase in the torch travel speed for all three values of the peak current. Therefore, in this work 3.5 A as peak current and for torch travel speed equal to 250 mm/min yielded higher joint strength. This is due to the fact that higher peak current gives more heat input which results in higher temperature of weld length thereby increasing HAZ, chances of oxidation, inclusion, porosity which are responsible for reduction in joint strength. It may also leads to excessive melting which results in burn through and undercut which also lowers joints strength. Higher torch travel speed leads to higher cooling rate allowing formation of finer grains which results in increase in joint strength.

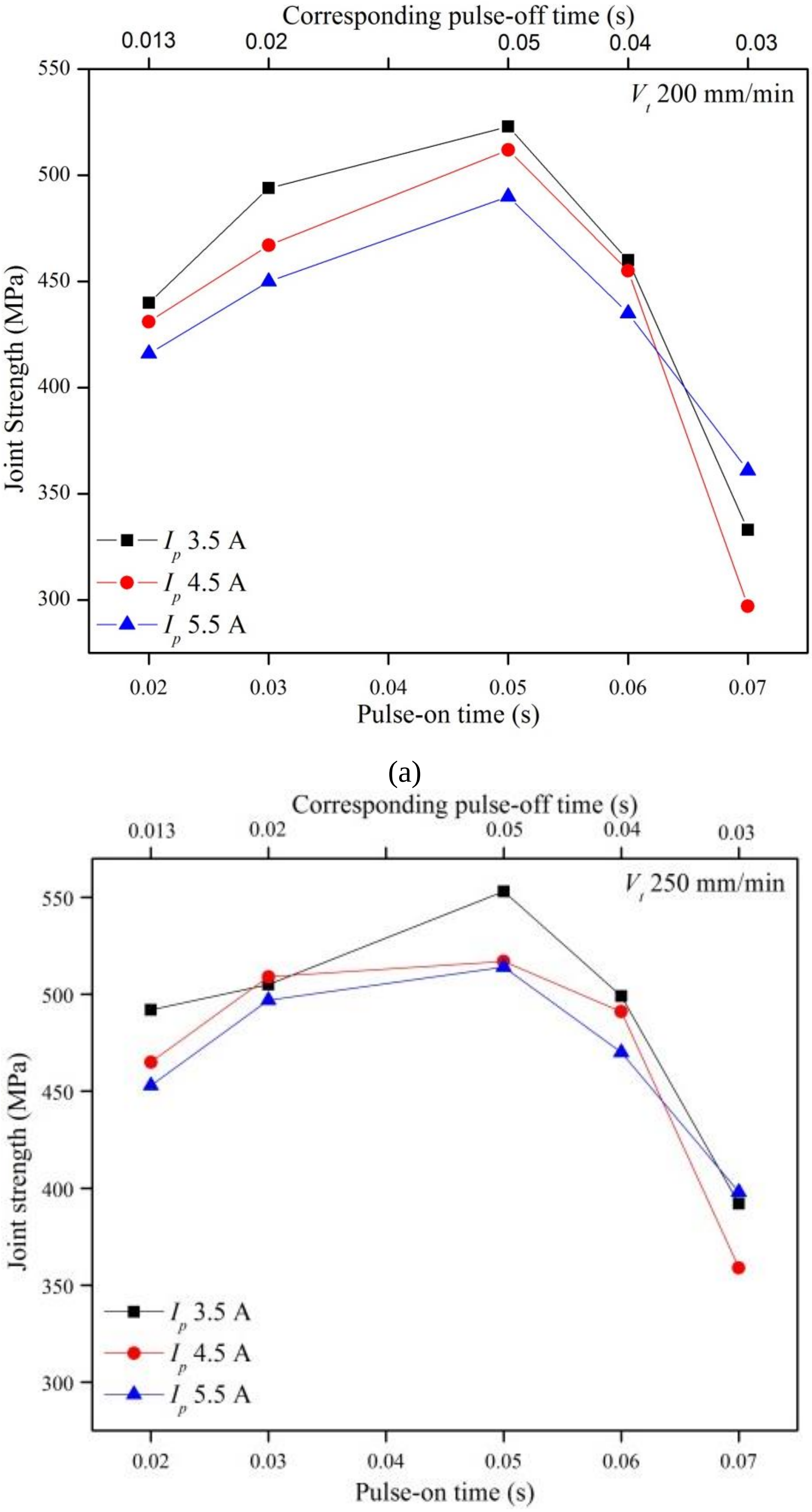

(a)

(b)

Fig. 4.1: Variation of joint strength with pulse-on time for torch travel speed of (a) 200; and (b) 250 mm/min. [NB: corresponding pulse-off times are also shown.]

Fig. 4.2 (a) and 4.2 (b) illustrate the variation of the joint strength with pulse-off time for torch travel speed equal to 200 mm/min and 250 mm/min respectively. The corresponding pulse-off time is shown on the top of figure respectively. It can be seen in both the figures that the minimum value of joint strength occurs at T_{off} equal to 0.03 s and with T_{on} at 0.07 s (corresponding to duty cycle of 70 % and pulse frequency of 10 Hz) whereas maximum joint strength occurs at T_{off} and T_{on} equal to 0.05 s for all three values of peak current and both torch travel speeds. Minimum yield of joint strength at T_{off} equal to 0.03 s and T_{on} at 0.07 s, this may be because lesser heat is dissipated during solidification and large heat conduction during melting time which results in increasing heat input and produces coarse grain size.

Fig. 4.3 (a) and (b) shows pulse-on time to pulse-off time ratio for torch travel speed 200 mm/min and 250 mm/min respectively. It was found that joint strength is maximum for pulse-on time to pulse-off time ratio equal to 1 and decreases with increase in pulse-on time to pulse-off time ratio. This reveals equal time for melting and solidification required for good joint strength.

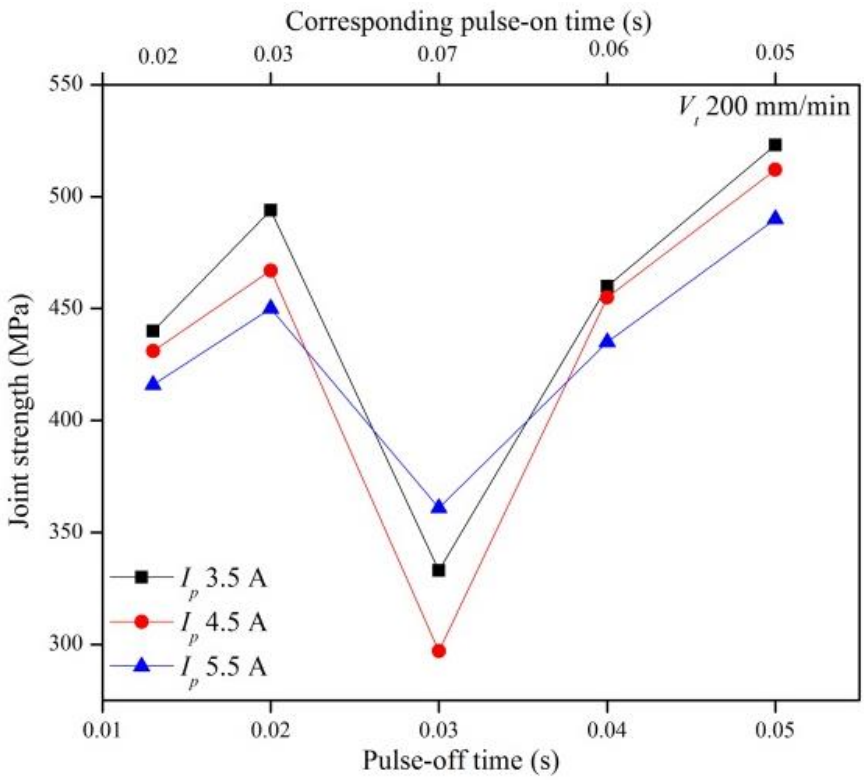

(a)

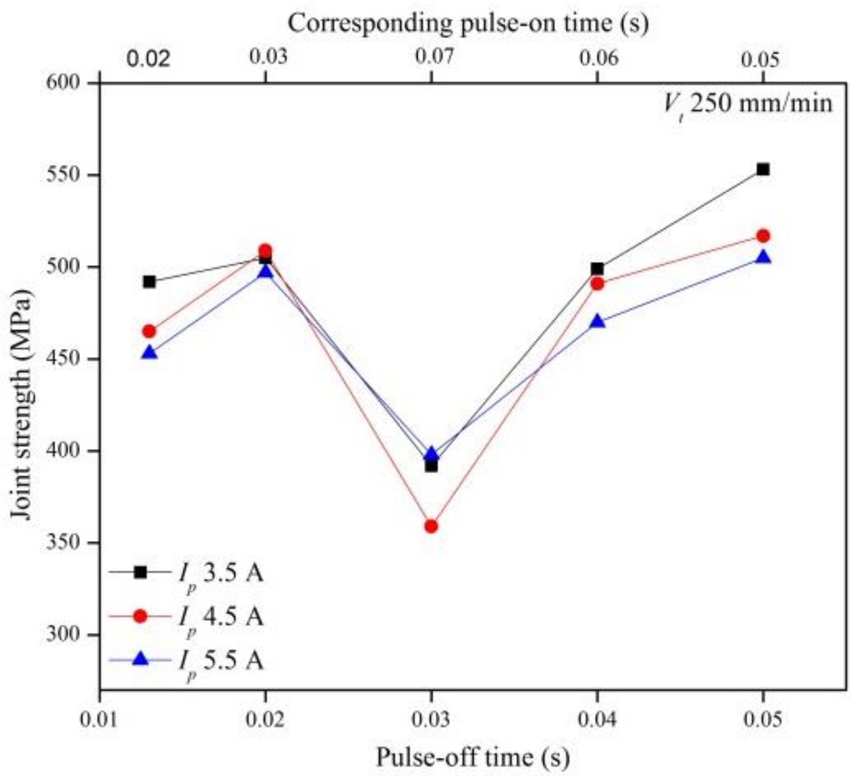

(b)

Fig. 4.2: Variation of joint strength with pulse-off time for torch travel speed of (a) 200 mm/min.; and (b) 250 mm/min. Corresponding pulse-on time are also shown.

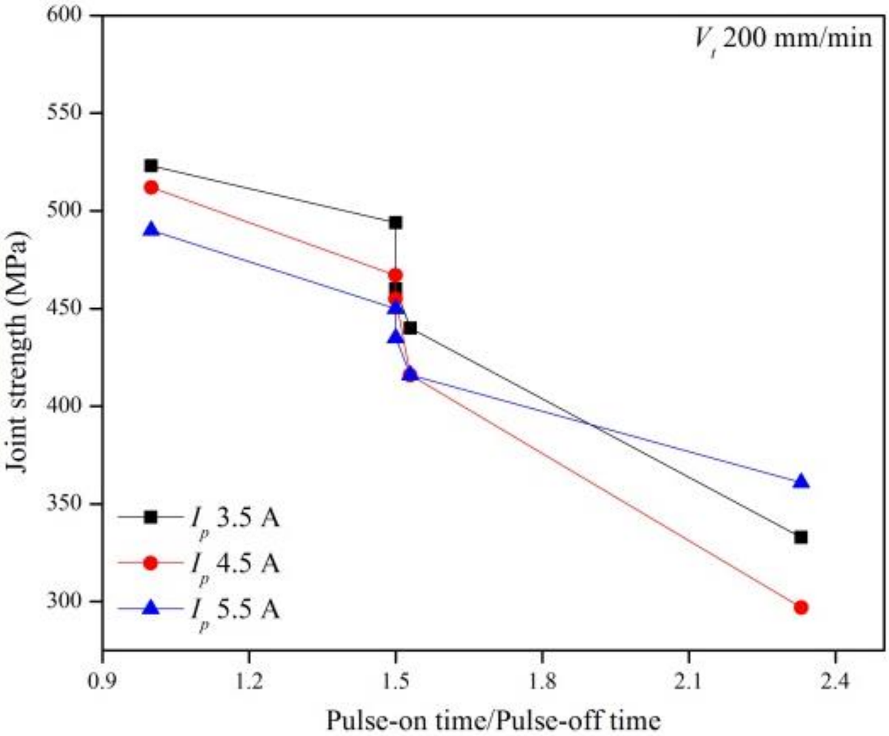

(a)

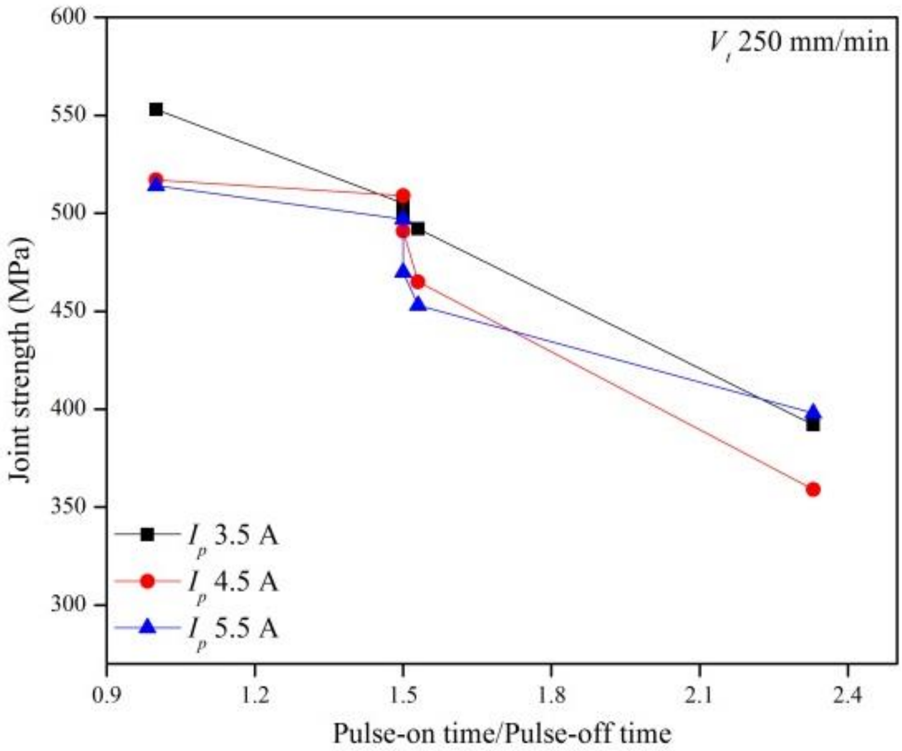

(b)

Fig. 4.3: Variation of joint strength with ratio of pulse-on time to pulse-off time for torch travel speed of (a) 200 mm/min; and (b) 250 mm/min

4.2 Microstructure

Microstructure of base material and fusion zone for optimal joint of the SS thin sheets obtained at peak current 3.5 A, pulse-on time 0.05 s, pulse-off time 0.05 s and torch travel speed 250 mm/min are shown in fig. 4.4 (a) and (b) respectively. The grain refinement in the fusion zone of the joint is the major consequence for higher tensile strength of the joint. It can be seen from this figure that planar grain structure of the base material transforms to the cellular structure in the fusion zone due to repeated heating and cooling during pulse-on and pulse-off times respectively. Fig. 4.4 (c), shows insignificant HAZ having dendritic structure with very small thermal distortion. These are responsible for 5% reduction in the ultimate tensile strength of the optimized joint to 553 MPa from ultimate tensile strength of the base material (582 MPa). This reduction in ultimate tensile strength is very small as compared to the conventional fusion welding processes. Grain refinement in the fusion zone of the joint is main reason for very small change in the ultimate tensile strength of the joint as compared to that of the base material.

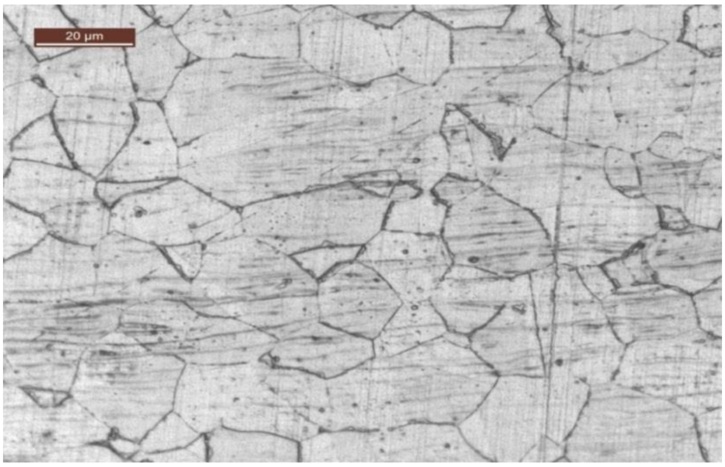

(a)

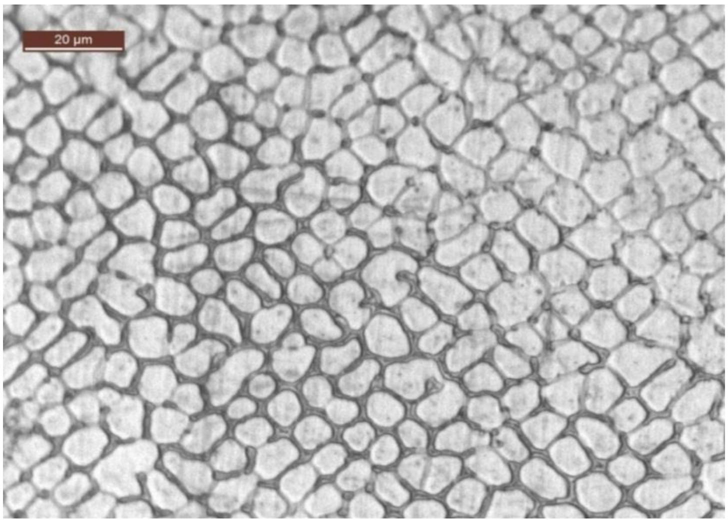

(b)

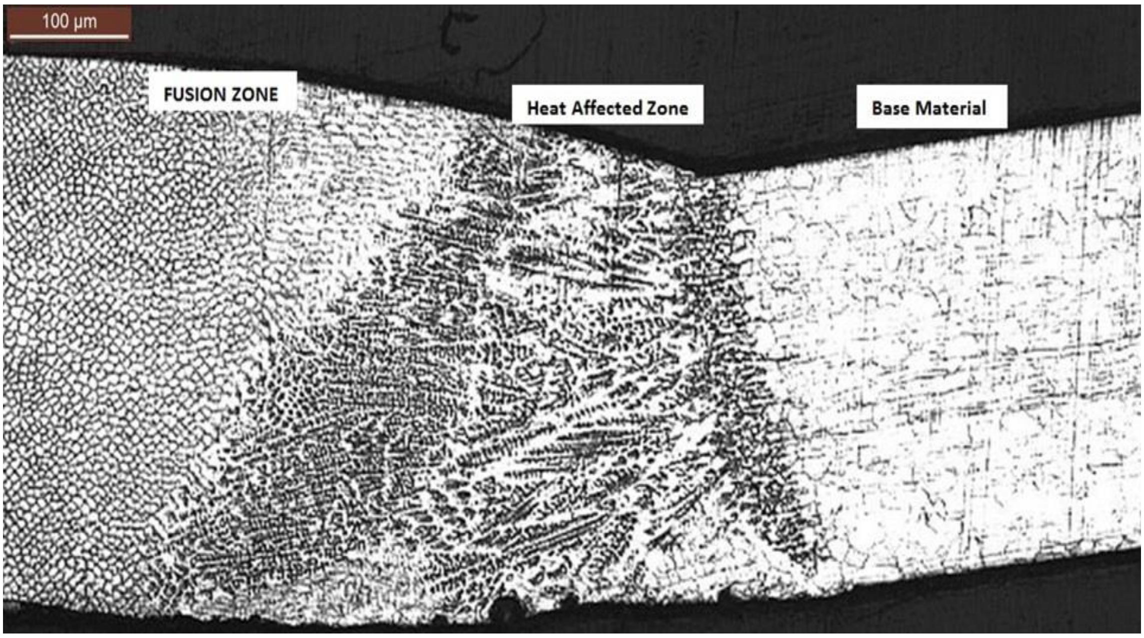

(c)

Fig. 4.4: Microstructure showing the microstructure of (a) base material; (b) fusion zone of optimized joint (at 50 X); and (c) joint showing fusion zone, HAZ and base material microstructure (at 20 X).

4.3 Microhardness

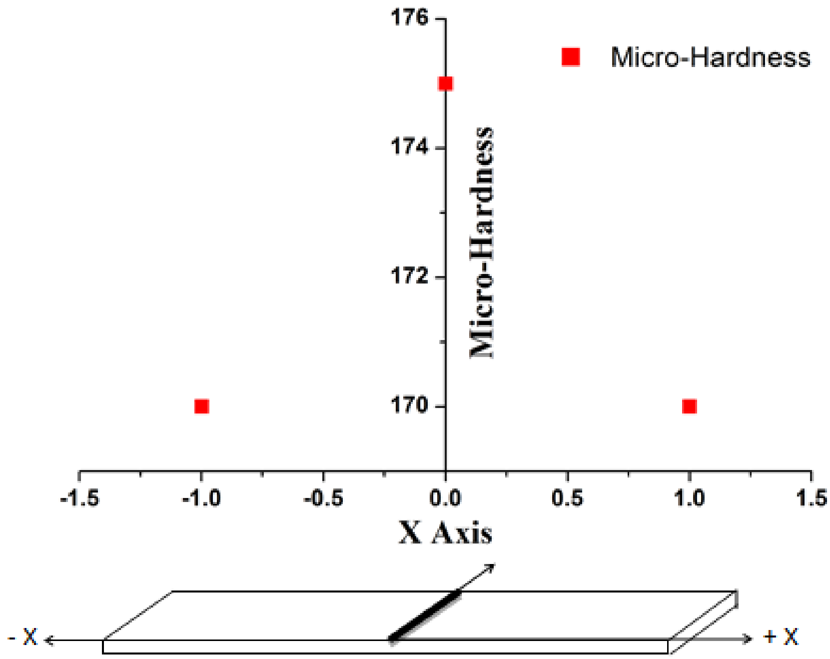

Fig. 4.5: Microhardness in longitudinal section in different positions.

Three consecutive micro-hardness measurements were taken for base material and its average micro-hardness was found to be 162.6HV0.2.The micro hardness for the optimal joint was measured across the longitudinal section of joint. Fig. 4.5 shows the location for hardness measurement. The variation in hardness across the joint is found to be 3% from the central value. Microhardness of the joint is found to be 7.6 % more than the microhardness of the base material. This suggests the absence of HAZ within the range of experimental parameters. This observation appears to be valid when one considers the narrow dimension of plasma beam.

4.4 Results of Analysis of Variance (ANOVA)

Analysis of variance (ANOVA) was conducted to determine the contribution of each process parameter and their interaction in influencing the joint strength. It also provides an indication of which process parameters are statistically significant. The result of ANOVA is shown in Table 4.2. ANOVA analysis was carried out for 95% confidence interval i.e. P values lower than 0.05 are considered to have significant effect on joint strength. The P-values test the statistical significance of each of the factors.

From Table 4.2, it can be seen that peak current (I_p), pulse-on time (T_{on}) and torch travel speed (V_t) and interaction of peak current with pulse-on time have significant influence on joint strength of thin SS sheets. It is worth-mentioning that the ANOVA analysis was done using I_p, T_{on}, V_t as factors however instead of T_{on}, if T_{off} is considered then again same ANOVA results are obtained. Hence, T_{off} is also equally significant as T_{on}.

Table 4.2: Results of ANOVA for joint strength.

Source	*D.F.*	SS	MS	*F*	*P*
Peak current	2	2618.5	1309.2	12.69	0.003
Pulse-on time	4	89322.9	22330.7	216.42	0.000
Torch travel speed	1	10083.3	10083.3	97.72	0.000
Peak current*Pulse-on time	8	3944.5	493.1	4.78	0.020
Peak current*Torch travel speed	2	8.9	4.4	0.04	0.958
Pulse-on time * Torch travel speed	4	862.3	215.6	2.09	0.174
Error	8	862.5	103.2		
Total	29	107665.9			

D.F. degree of freedom, SS sum of squares, MS mean squares ,*F F* value , *P P* value

Chapter 5

Conclusions and Scope of Future Work

This chapter summarizes the significant achievements and conclusions from the present work highlighting the extent to which the aims and objectives are met. It also presents the possibilities for future work based on the outcomes of the research.

5.1 Conclusions

Influence of pulsed parameter peak current, pulse-on time, torch travel speed on joint strength of 0.4 mm thin sheets of SS 316L have been studied. Following conclusion can be drawn from the present research work:

1. Use of continuous power supply resulted in large heat causing burn through even at very low value of current of 0.9 A. Based on these observation it was decided to use pulse power supply for joining thin sheets of stainless steel.
2. To achieve uniform fusion in thin sheet material, i.e. without burn-through, it is essential that the component edges are accurately machined and that the clamping provides a uniform heat sink. It is also necessary to ensure that the two faces are in perfect contact along the entire length of the joint.
3. Pulse micro-plasma transferred arc process has capability of joining thin sheets of SS producing joint with insignificant HAZ, thermal distortion, porosity and consuming very less amount of current and power. This process proves to be highly energy efficient process.
4. Optimum values of pulse-on time, pulse-off time, peak current, and torch travel speed exist to maximize the joint strength. The identified optimum values of these parameters are 0.05 s; 0.05 s (i.e. duty cycle of 50%); 3.5 A; and 250 mm/min. respectively yielding maximum value of joint strength as 553 MPa.
5. For a particular combination of pulse-on time and pulse-off time, the joint strength increases with increasing value of torch travel speed and with decrease in peak current.
6. Attainment of maximum joint strength at equal values of pulse-on and pulse-off times indicates significance of balance between the times available for melting, fusion and solidification of sheet material to yield a high strength and quality of the sheet joint.
7. Maximum joint strength was achieved when pulse-on time to pulse-off time ratio is 1. Equal time for melting and solidification required for good joint strength.

8. Increasing pulse-on time to pulse-off time ratio more than one results in decreased joint strength.
9. Grain refinement in fusion zone is mainly responsible for increase in the joint strength.
10. Change of microhardness from base material to joint is negligible which results in insignificant HAZ.

5.2 Scope for the Future Work

- Automated wire feeder could be used to achieve higher strength than the base material.
- Aspect ratio of bead geometry can be correlated to the joint strength.
- One can design and perform experiments with back side of shielding (back purging) to reduce the chances of oxidation and porosity.
- Thermocouple and thermal camera may be used for thermal analysis.
- Pulsed μ-PTA joining process can be explored for joining even thinner sheets of stainless steel and other corrosion and wear resistant materials such as super alloys, titanium based alloys, etc.

References

1. **American Welding Society**, Welding Handbook, 9th. Ed., Miami.
2. **Ananth, M.G., Babu, B.S., Chakravarthy, P., Jayakumar, K., Manickavasagam, A., Arunprakash, N.V.S., Gopalakrishnan, K.M. (2013)**, Experimental investigations on electron beam welding of austenitic / ferritic stainless steel for space applications. *International Journal of Research in Mechanical Engineering & Technology*, 3(2), 45-50.
3. **Balasubramanian, M., Jayabalan, V., Balasubramanian,V. (2008a),** Effect of microstructure on impact toughness of pulsed current GTA welded α–β titanium alloy. *Materials Letters.* 62, 1102–1106.
4. **Balasubramanian, M, Jayabalan. V., Balasubramanian, V. (2008b)**, Process parameter optimization of the pulsed current argon tungsten arc welding of titanium alloy. *Journal of Material Science and Technology,* 24(3), 423-426.
5. **Balasubramanian, M., Jayabalan, V., Balasubramanian, V. (2010)**, Effect of process parameters of pulsed current tungsten inert gas welding on weld pool geometry of titanium welds. *Acta Metalugica Sinica (English Letter)* 23 (4) 312-320.
6. **Dean, G., Norrish, J., Cook, C. (2005)**, Evaluation of control techniques for dip transfer gas metal arc welding *Australasian Welding Journal* 50, 213-221.
7. **Farid, M., Molian, P.A. (2000)**, High-brightness laser welding of thin sheets of 316 stainless steel. *Journal of Materials Science* 35, 3817-3826.
8. **Jhavar, S.; Paul, C.P.; Jain, N.K. (2014)**, Development of micro-plasma transferred arc (μPTA) wire deposition process for additive layer manufacturing applications. *Journal of Materials Processing Technology*, 214(5), 1102-1110.
9. **Javidrad, F., Rahmati, R. (2009)**, An integrated re-engineering plan for the manufacturing of aerospace components. *Materials and Design* 30, 1524–1532.
10. **Juang, S.C., Tarng, Y.S. (2002)**, Process parameter selection for optimizing the weld pool geometry in the tungsten inert gas welding of stainless steel. *Journal of Materials Processing Technology.* 122, 33–37.
11. **Karimzadeh, F, Salehi, M., Saatchi, A., Meratian, M. (2005)**, Effect of micro-plasma arc welding process parameters on grain growth and porosity distribution of thin sheet Ti6Al4v alloy weldment. *Materials and Manufacturing Processes*, 20,205–219.

12. **Karadeniz, E., Ozsarac, U., Yildiz, C. (2007)**, The effect of process parameters on penetration in gas metal arc welding processes. *Materials and Design* 28, 649–656.
13. **Kim, C., Choi, W., Kim, J., Rhee, S. (2008)**, Relationship between the weldability and the process parameters for laser-TIG hybrid welding of galvanized steel sheets. *Materials Transactions*, 49(1) 179-186.
14. **Klimpel, A., Lisiecki, A. (2007)**, Laser welding of butt joints of austenitic stainless steel AISI 321. *Journal of Achievements in Materials and Manufacturing Engineering*, 25(1) 63-66.
15. **Kumar, A., Sundarrajan, S. (2008)**, Optimization of pulsed TIG welding process parameters on mechanical properties of AA 5456 aluminum alloy weldments. *Materials and Design*, 30, 1288–1297.
16. **Kumar, R., Dilthey, U., Dwivedi, D.K.; Sharma, S.P., Ghosh, P. K**. **(2009)**, Welding of thin sheet of Al alloy (6082) by using vario wire DC P-GMAW. *International Journal of Advanced Manufacturing Technology* 42,102–117.
17. **Kumar, P., Datta, C.K. (2012)**, Pulsed parameters optimization of GTAW process for mechanical properties of Ti-6Al-4V alloy using Taguchi method, *International Journal of Engineering Science and Innovative Technology* ,1(1), 75-80.
18. **Kumar, D., Elangovan, S., Shanmugan, S. (2014)**, Parametric optimization of pulsed-TIG welding process in butt joining of 304l austenitic stainless steel sheets. *International Journal of Research in Engineering and Technology,* 3 (11), 213-219.
19. **Kou, S**. (2003), **Welding Metallurgy**, *John Wiley & Sons, New Jersey*.
20. **Liu, M. Y., Shi, B., Wang, C., Ji, S. K., Cai, X., Song, H. W. (2003)**, Normal hall-peach behavior of mild steel with submicron grains. *Material Letters*, 57-19, 2798-2802.
21. **Mirakhorli, F., Ghaini, F.M., Torkamany, M.J. (2012)**, Development of weld metal microstructures in pulsed laser welding of duplex stainless steel. *Journal of Materials Engineering and Performance*, 21, 2173–2176.
22. **Masoumil, M. Marashi2, S.P.H., Pouranvari, M. (2009)**, Assessment of the effect of laser spot welding parameters on the joint quality using Taguchi method. *Metal*, 1- 9.

23. **Okamoto, Y., Gillner, A., Olowinsky, A., Gedicke, J., Uno, Y. (2008)**, Fine micro-welding of thin stainless steel sheet by high speed laser scanning. *Journal of Laser Micro/NanoEngineering*3, (2), 95-99.
24. **Piccini, J., Svoboda, J. (2012)**, Effect of the plasma arc welding procedure on mechanical properties of DP700 steel. *Procedia Materials Science* 1, 50 – 57.
25. **Prasad, K.S., Rao, C.S., Rao, D.N. (2011a)**, Prediction of weld pool geometry in pulsed current micro plasma arc welding of SS304L stainless steel sheets. *International Transaction Journal of Engineering, Management, & Applied Sciences & Technologies*, 2, 325-336.
26. **Prasad, K.S., Rao, C.S., Rao, D.N. (2011b)**, A study on weld quality characteristics of pulsed current micro plasma arc welding of SS304L sheets. *International Transaction Journal of Engineering, Management, & Applied Sciences & Technologies*, 2, 437-446.
27. **Prasad, K.S., Rao, C.S., Rao, D.N. (2012a)**, Study of pulsed micro plasma arc welding parameters on weld bead geometry of AISI 304L sheets using factorial method. *International Journal of Science and Technology*, 17, 31-41.
28. **Prasad, K.S., Rao, C.S., Rao, D.N. (2012b)**, Study on factors affecting weld pool geometry of pulsed current micro plasma arc welded AISI 304L austenitic stainless steel sheets using statistical approach. *Journal of Minerals and Materials Characterization and Engineering*, 11, 790-799.
29. **Prasad, K.S., Rao, C.S., Rao, D.N. (2012c)**, Establishing empirical relations to predict grain size and hardness of pulsed current micro plasma arc welded SS 304L sheets. *American Transactions on Engineering & Applied Sciences,* 1, 57-63.
30. **Prasad, K.S., Rao, C.S., Rao, D.N. (2012d)**, Optimizing fusion zone grain size and ultimate tensile strength of pulsed current micro plasma arc welded Inconel 625 alloy sheets using Hooke & Jeeves Method. *International Transaction Journal of Engineering, Management, & Applied Sciences & Technologies,* 3, 87-100.
31. **Prasad, K.S., Rao, C.S., Rao, D.N. (2013)**, Application of grey relational analysis for optimizing weld bead geometry parameters of pulsed current micro plasma arc welded AISI 304L stainless steel sheets, *International Journal of Advanced Design and Manufacturing Technology,* 6, 79-86.
32. **Rao, C.S., Prasad, K.S., Rao, D.N. (2012),** Study on effect of welding speed on micro structure and mechanical properties of pulsed current micro plasma arc

welded Inconel 625 sheets. *Journal of Minerals and Materials Characterization and Engineering*, 11, 1027-1033.

33. **Tarng, Y.S, Yang, W.H. (1998)**, Optimization of the weld bead geometry in gas tungsten arc welding by the Taguchi method. *The International Journal of Advanced Manufacturing Technology*, 14, 549-554.
34. **Tarng, Y.S., Tsai, H.L., Yeh, S.S. (1999)**, Modeling, optimization and classification of weld quality in tungsten inert gas welding, *International Journal of Machine Tools & Manufacture* 39, 1427–1438.
35. **Tseng, K.H., Hsieh, S.T., Tseng, C.C. (2003)**, Effect of process parameters of micro-plasma arc welding on morphology and quality in stainless steel edge joint welds. *Science and Technology of welding and joining*, 8,423-430.
36. **Urena, A, Otero, E., Utrilla, M.V., Munez, C.J. (2007)**, Weldability of a 2205 duplex stainless steel using plasma arc welding. *Journal of Materials Processing Technology*, 182,624–631.
37. **Ventrella, V.A., Berretta, J.R., Rossi, W.D. (2010)**, Pulsed Nd: YAG laser beam welding of AISI 316L stainless steel thin foils. *Journal of Materials Processing Technology* 210, 1838–1843.
38. **Yilbas, B.S., Arif, A.F.M., Aleem, B.J.A. (2010)**, Laser welding of low carbon steel and thermal stress analysis. *Optics & Laser Technology* 42, 760–768.
39. **Zhang, D.K., Niu, J.T. (2000)**, Application of artificial neural network modeling to plasma arc welding of aluminum alloys. *Journal of Advanced Metallurgical Sciences*, 13, 194-200.

Appendix-A: Detail of the instrument used

- **Leica inverted microscope**

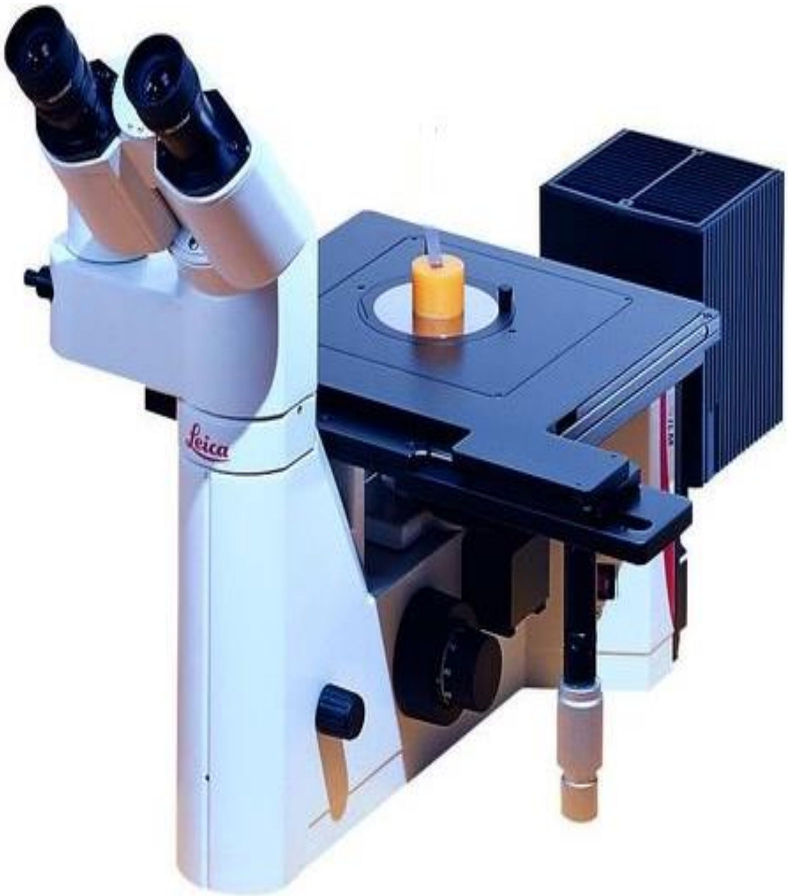

Make	**Leica Microsystems, *Germany***
Model	*DMIL*
Optics	Leica HC optics (infinity corrected) HC objectives: 2.5x-100x
Transmitted-Light Illuminator	5 watt LED, external power supply (in 100-240, out 5V/2A) Filter holder for TL filter Ø 32mm, collector, scattering filter
Focus	Coaxial coarse and fine adjustment, travel path 7 mm, nosepiece focusing

- **Vickers Microhardness Tester**

Make	**Walter UHL*TechnischeMikroskopie GmBH, Germany***
Model	*VMH002 V*
Load Range	1 grams-2000 grams
Type of Indenter	Diamonds square base hexagonal pyramid

- **Tensile Testing Machine**

Make	***Tinius Olsen USA***
Model	*Tinius Olsen H50KL*
Load Range	1-50 kN
Clearance Between Columns	405 mm
Testing Speed Range	0.001 to 500 mm/min